ASSESSMENT OF THE THERMAL AND ENERGY PERFORMANCE OF PHOTOVOLTAIC MODULES IN AGRIVOLTAIC SYSTEMS

A THESIS SUBMITTED IN PARTIAL FULFILMENT OF THE

REQUIREMENTS FOR THE DEGREE OF

MASTER OF SCIENCE IN RENEWABLE ENERGY

OF

THE UNIVERSITY OF NAMIBIA

BY

HERTHA LIINA MBALUNDU

201704841

APRIL 2025

MAIN SUPERVISOR: DR. PETJA DOBREVA

(UNIVERSITY OF NAMIBIA)

CO-SUPERVISOR: DR.-ING MATTHEW BERWIND

(FRAUNHOFER INSTITUTE FOR SOLAR ENERGY SYSTEMS ISE)

Abstract

The study evaluates the thermal and energy performance of photovoltaic modules in an agrivoltaic system in Benin, west Africa. This was done by employing three sets of heat transfer coefficients: Faiman, Benin, and Büren into the Faiman module-temperature prediction model. The dataset for this study extends from April to July 2023, marked by high ambient temperatures exceeding 30℃. According to the findings, the cooling effect was significant for the results of Büren coefficients, and the agrivoltaic system generated up to 3.0% more energy than the non-agrivoltaic, especially at higher module temperature ranges of 40 ℃ - 55 ℃. The Benin coefficients demonstrated a moderate cooling effect, evidenced by a positive energy yield difference of up to 1.0% in the month of May. However, the cooling effect reduced in the hotter month of July resulting in a -1.0% energy difference between the two systems. The Faiman coefficient, on the other hand, demonstrated no cooling effect, as shown by consistently yielding negative energy differences, especially in May (-1.0%).

The statistical analysis indicates that the Faiman coefficients provided a closer fit to the actual Benin-derived temperatures (R^2: 0.99 and MAE: 0.54 ℃). Whereas the results from the Büren coefficients showed the strongest cooling effect, achieving a reduction in module temperatures of up to 4℃ relative to the non-agrivoltaic system. The findings highlight the need for site-specific coefficient tuning to enhance the accuracy and the reliability of the findings.

Keywords: Agrivoltaic (APV), Photovoltaic (PV), Thermal Analysis, Cooling Effects, Integrated PV

List of Publication/ Conferences/ Proceedings

This work was presented via poster exhibition at the “JCol Youth for Green Hydrogen (Y4GH2) Scholarship Programme Visibility Event” held in Berlin on September 11, 2024. The event was organised by SASSCAL, and it focused on the advancements made regarding the Joint Communique of Intent (JCol) signed between Namibia and Germany in 2021, which supports Namibia’s Green Hydrogen initiatives. The event provided an opportunity for master’s students in the Y4GH2 program to present their research and connect with industry experts, academic leaders, and policymakers in the Green Hydrogen sector.

.

Table of content

List of Tables

List of Figures

Acknowledgement

- I would like to express my deepest gratitude to my supervisors, Dr. Petja Dobreva, Dr. Ing. Matthew Berwind, and Mr. Richmond Kuleape, for their tireless guidance, support, and encouragement throughout this research.
- I would also like to extend my heartfelt appreciation to Monica Anis Nicola for her unwavering support and guidance throughout this work.
- I am deeply thankful to Fraunhofer ISE for providing me with the opportunity, necessary datasets, and facilities to conduct this work.
- I would also like to give a special thanks to Sasscal for their financial support, which allowed me to carry out all the work.
- A special thank you also to my family for your love and support during this period.
- Most importantly, I would like to give thanks to the Almighty God for the blessing of life and for being with me until I completed the thesis; it would not have been possible without him.

Dedication

This thesis is wholeheartedly dedicated to my beloved late father, Mr. Festus Mbalundu, who was my greatest source of support and encouragement. Your absence has left an irreplaceable void, but your love and guidance continue to shape me into a strong girl. You were always there throughout my life and most importantly my academic journey, and it deeply hurts that you are not here to celebrate this milestone with me. I know you are watching over me with pride and joy. I miss you dearly, Daddy. Until we meet again!

Declaration

I, Hertha Liina Mbalundu, hereby declare that this study is my own work and is a true reflection of my research, and that this work, or any part thereof has not been submitted for a degree at any other institution. No part of this thesis may be reproduced, stored in any retrieval system, or transmitted in any form, or by means (e.g. electronic, mechanical, photocopying, recording or otherwise) without the prior permission of the author, or The University of Namibia in that behalf. I, Hertha Liina Mbalundu, grant The University of Namibia the right to reproduce this thesis in whole or in part, in any manner or format, which The University of Namibia may deem fit.

Hertha L. Mbalundu	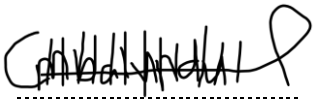	April 2025
Name of Student	Signature	Date

Chapter 1: Introduction

1.1. Background of the study

The world population increases each year and is projected to continue increasing in the next decades [1,2]. This results into land-use conflict for agriculture, power plants and other infrastructures due to an increase in basic needs such as energy, shelter, and food. Over the years, the energy sector has been dominated by fossil fuels which contribute to global warming [3]. In addition, the International Energy Agency (IEA) [4] and other sources [5,6] indicated that the energy sector contributes around 73% to the global greenhouse gas (GHG) emission. Therefore, there is a need to transition to cleaner sources of energy such as the photovoltaic (PV) technology.

PV technology is a widely adopted renewable energy solution that directly convert sunlight into electricity, providing a sustainable substitute of fossil fuels [7]. As nations strive for renewable energy adoption goals to combat climate change, the large-scale deployment of PV systems has grown significantly. In addition, the IEA has projected that about 6000TWh will be generated from PV by 2050 [8]. Nonetheless, a primary problem linked to the widespread PV installation is the enormous land requirement [9], which sometimes results in land-use conflicts, especially in countries where arable land is limited [10]. This issue is exacerbated by the heat island effect, wherein, large-scale PV installations may cause raised local temperature due to heat absorption and restricted cooling mechanisms, as per the findings of Barron-Gafford et al. [11].

Innovative strategies are being explored to enhance land use efficiency by integrating PV systems with alternative land uses, including agriculture. This method, referred to as

agrivoltaic, entails the simultaneous use of PV panels and crops on the same piece of land for energy generation and crop production as shown in Figure 1.1. This dual-use strategy is becoming increasingly significant as it has the potential to minimise land-use conflicts, enhance land productivity, and promote the sustainability objectives of various sectors e.g. the energy and agriculture sectors.

Figure 1.1: Agrivoltaic system in Kressbonn, Germany [12]

A notable undesirable property of PV technology is the temperature sensitivity of solar panels. As solar cells / PV panels increase in temperature, their power generation capacity considerably reduces. The reduction in the power output can go up to 0.5% for every degree rise in temperature, when the temperatures are above 25℃ [13,14]. This reduction in efficiency is typically due to the thermal properties of the PV materials, wherein the higher temperatures result in increased resistive losses and a decrease in output voltage. Consequently, regulating the thermal conditions of PV panels is essential for sustaining their performance, especially in areas with high ambient temperatures.

The temperature sensitivity issue of PV modules could potentially be improved by the concept of agrivoltaic. This unique arrangement results in a shared light environment where the solar panels positioned above a portion of the crop, cast shadows, and subsequently create a distinct microclimate in the growing area [15,16]. This shift in microclimatic conditions can have implications on the operating temperature of PV panels [17]. Therefore, it is important to determine the effect of the microclimate changes on the operating temperatures of PV modules in agrivoltaic systems.

For example a study Williams et al. [18] in the United States found that the temperature of PV modules in an agrivoltaic system mounted at 4m high were found to be 10℃ cooler compared to PV modules mounted at 0.5m on bare soil. Similarly, another study in the United States by Barron et al. found that the air temperature within the microclimate of Agrivoltaic system were about 1.2℃ cooler during the day compared to the air temperature in non-Agrivoltaic systems [15]. More studies such as [15–17,19] were also able to show how strongly crops and modules can influence the microclimate in Agrivoltaic systems.

Although a few studies have recognized the potential cooling effect of Agrivoltaic systems on PV modules in one type of conditions such as the USA, these findings may not be valid in other conditions. In addition, the degree of cooling has not been extensively investigated yet especially in conditions such as tropical climates. A significant number of research is focused more on assessing the impact of microclimate on crop yield and less focus on the yield of PV modules in agrivoltaic systems. It is important to investigate the thermal performance of modules in agrivoltaic systems due to the significant effect it has on the power output of PV modules. To achieve this aim, it is necessary to understand the

photovoltaic theory, module temperature prediction models and most importantly the microclimatic changes in Agrivoltaic systems.

Therefore, the study aims to assess whether PV modules in agrivoltaic systems experience lower temperatures due to the influence of plants as hypothesised by numerous studies.

1.2. Statement of the problem / Motivation

The temperature of PV panels increases during operation, which significantly reduce the output power of the panels by up to 0.5% for each degree increase in temperature above 25℃. The presence of crops in agrivoltaic systems could potentially lead to cooler PV panels which could result in improved energy production. However, this cooling effect remains uncertain in most of the studies as it has not been extensively investigated, especially in various climate conditions.

In addition, there are not many agrivoltaic plants globally that can provide experimental data to assess the effectiveness of the cooling effect due to the presence of crops underneath the PV panels. It is also possible that the heat flux mechanisms and microclimate formation in some climates may not replicate the cooling benefits as observed in some regions.

1.3. Objectives of the study / Purpose

The goal of the study was to assess whether the integration of crops underneath the PV panels in agrivoltaic systems potentially results in any cooling effect in comparison to non-agrivoltaic systems. The term non-agrivoltaic system in this study refers to the

conventionally installed PV plants without crops underneath the panels. The study also aims to quantify the extend of the cooling effect (if any) and analyse the resulting energy performance of the panels within the two systems. The analysis was done using the reference dataset obtained from an agrivoltaic system in Benin, West Africa, which has a tropical climate condition. This goal was achieved by realising the following objectives:

a. Predict the operating temperature of PV modules in agrivoltaic systems and non-agrivoltaic installations using a suitable model for predicting module temperatures.
b. Analyse the thermal performance of PV modules in agrivoltaic systems compared to PV modules in non-agrivoltaic systems.
c. Investigate whether PV modules in agrivoltaic systems experience lower temperatures and quantify the extent of any cooling effect.
d. Assess and compare the impact of thermal performance on the energy output of PV modules in both Agrivoltaic and non-Agrivoltaic systems.

1.4. Thesis layout

Chapter 2 provides a comprehensive overview of the Agrivoltaic concept, including the potential opportunities, and constraints associated with the implementation of Agrivoltaic systems. The photovoltaic theory, which explains how electricity is produced in a solar cell, is covered in chapter 3. The variations on the I-V curve are used in this section to further illustrate how the external factor (the microclimate in this case) affect the performance of PV module. This section also analyses the causes and heating effects in solar modules. Chapter 4 compares various module temperature prediction models. The causes and impacts of heat in a module are also analysed and the possible cooling

techniques are outlined. Chapter 5 outlines the location where data was collected, the type of data collected and how it was collected. It also describes the tools used to analyse and how the data was analysed. The modelling of PV panel temperature and tuning heat transfer coefficients are discussed in Chapter 6. Furthermore, Chapter 7 lists and discusses the results obtained. It connects the findings of the literature and scientific theories to analyse the data. Lastly, chapter 8 draws conclusion and make recommendation respectively.

Chapter 2: Agrivoltaics systems

2.1. Overview and development of agrivoltaic

Agrivoltaic involves the simultaneous use of land for both agricultural practices and the generation of PV solar energy [12]. As illustrated in Figure 2.1, agrivoltaic systems are categorised as either open or closed systems, with structures that range from interspace PV to opaque buildings. Typical applications include aquaculture, horticulture, arable farming, and grassland which produce staple foods and animal feed.

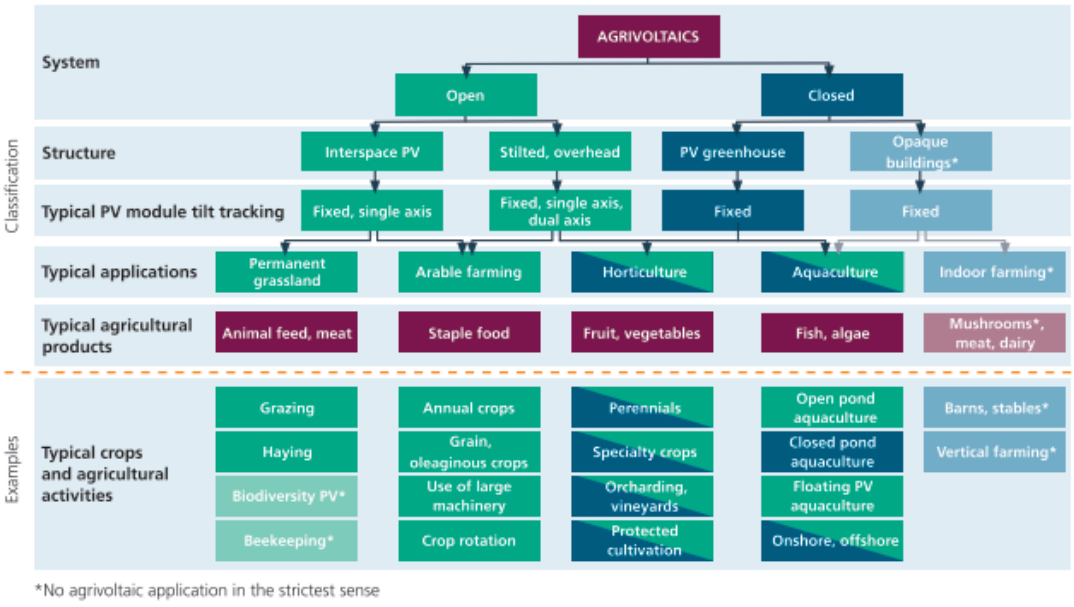

Figure 2.1:Classification of agrivoltaic systems [12]

Historically, the concept of Agrivoltaic was first proposed by Prof. Goetzberger (founder of Fraunhofer ISE) and Dr. Zastrow in 1981 as shown in Figure 2.2(A) [20]. The concept involves the elevation of PV modules up to 5m to allow crops to grow below the modules

as illustrated in Figure 2.2 (B) [12]. The vertical clearance of the module structures is typically determined by the type of crops to be grown and the agricultural machinery to be used [12]. The progression of agrivoltaic from limited trials to extensive initiatives has been influence by technological advancements, favourable polices, and an increasing demand for sustainable land management practices [21]. According to various reviews and reports, the technology has increased globally from $5MW_p$ in 2012 to more than $15GW_p$ in 2021 [12].

Figure 2.2: Sketch of the agrivoltaic idea in 1981 by Prof Goetzberger et al (A) [20]. Implementation of the agrivoltaic idea in real life systems (B) [12]

Advantages and possibilities of Agrivoltaic

Agrivoltaic presents a range of advantages and possibilities, positioning itself as an effective approach for maximizing land utilization, improving agricultural output, and producing renewable energy. The integration of solar energy generation with agricultural practices presents a strategic solution to the concurrent issues of fulfilling global energy requirements and maintaining sustainable food production. This section examines the ways in which Agrivoltaic can optimize land productivity, enhance resource efficiency, and contribute to the performance of PV modules.

- **Improving land productivity and resource utilisation**

As illustraed in Figure 2.3, agrivoltaic systems are engineered to optimize land productivity by facilitating concurrent agricultural activities and solar energy production. This dual-use approach optimizes land productivity and serves as a strategic solution for areas experiencing land-use conflicts or scarcity [12,21].

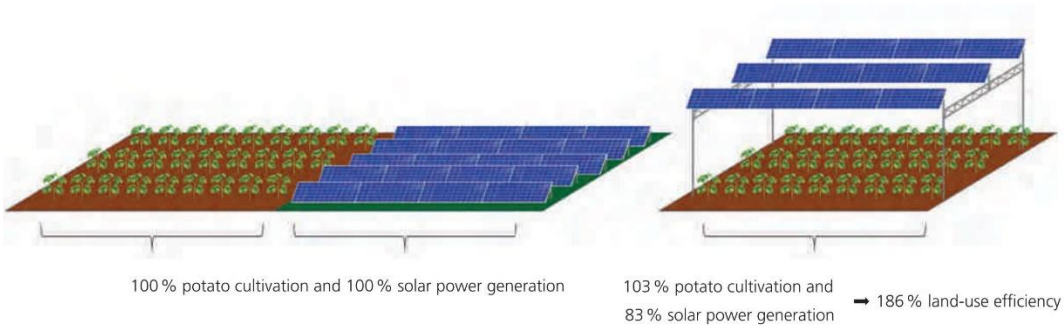

Figure 2.3: Dual use of land to promote land use efficiency [12].

- **Enhancing Land Equivalent Ratios (LER)**

The Land Equivalent Ratio (LER) quantifies the overall productivity of agricultural and energy outputs in agrivoltaic systems, relative to utilizing the same land area for a singular purpose [22]. An LER exceeding 1.0 signifies that the combined utilization of the land yields higher productivity compared to its individual use for agriculture or solar energy [12]. In a study conducted by Dupraz et al. [22] in southern France, it was observed that Agrivoltaic systems attained a Land Equivalent Ratio (LER) ranging from 1.35 to 1.70. This suggests that the overall productivity of the land increased by as much as 70% when crops and solar panels were used in conjunction. The precise value of the LER is contingent upon various factors, including:

- ✓ The performance of various crop types varies significantly based on light exposure. Leafy vegetables, including lettuce and spinach, generally thrive in partial shade, leading to increased Land Equivalent Ratios (LERs). In contrast, sun-loving crops like wheat and corn typically show reduced LERs under similar conditions.
- ✓ The configuration of the system, including the spacing, tilt angle, and height of the PV panels, plays a crucial role in determining the amount of light that reaches the crops and the resulting shading effects. These factors can have a substantial effect on both agricultural yields and energy generation [23].

Alongside the LER, the notion of solar sharing efficiency can be examined to assess the performance of agrivoltaic systems. The efficiency of solar sharing quantifies how effectively crops harness sunlight that is not directly transformed into electricity by solar panels. For example, agrivoltaic projects that utilize elevated PV arrays or adjustable panels can enhance solar sharing by modifying panel positions in response to crop requirements, thereby improving land productivity.

- **Enhancing Water Conservation and Optimizing Water Utilization**

Agrivoltaic systems offer a significant advantage in conserving water and enhancing water use efficiency within agricultural practices. The installation of solar panels establishes a microclimate that effectively lowers evapotranspiration rates by offering shade to the crops and keeping soil temperatures cooler. The decrease in evaporation is especially advantageous in arid and semi-arid areas, where the challenge of water scarcity is pronounced.

Research indicates that agrivoltaic systems can lead to a reduction in evapotranspiration rates up to 20% , influenced by factors such as climate, crop type, and panel configuration [15,21,24]. In dryland farming regions of Arizona, research indicated that the installation of PV panels led to a decrease in soil moisture loss. This facilitated the growth of crops like chili peppers and tomatoes, which required less irrigation than those grown in non-agrivoltaic fields. The capacity to conserve water via agrivoltaic effectively lowers agricultural production costs while simultaneously promoting sustainable farming practices by reducing the environmental consequences associated with water consumption.

- **Improved agricultural productivity and adaptability to changing climatic conditions**

Beyond conserving water, the partial shading effect of agrivoltaic systems offers advantages for crops by mitigating heat stress and safeguarding them from severe weather conditions, including hail, high winds, and intense solar radiation [12]. In areas characterized by elevated temperatures, the presence of solar panels provides shade that can reduce the surrounding ambient temperature for crops [25]. This reduction plays a significant role in alleviating heat stress and enhancing the crops' resilience to fluctuations in climate. This microclimate has the potential to establish a more advantageous environment for specific crops, which may result in increased yields and enhanced crop quality.

2.2. Microclimates in Agrivoltaic systems

As illustrated in Figure 2.4, microclimate refers to a localised climate conditions, such as temperature, humidity, wind speed and light levels, created under and around the solar modules in agrivoltaic systems [26]. Analysing the factors that affect microclimate formation and the subsequent advantages is crucial for enhancing the design and management of agrivoltaic systems.

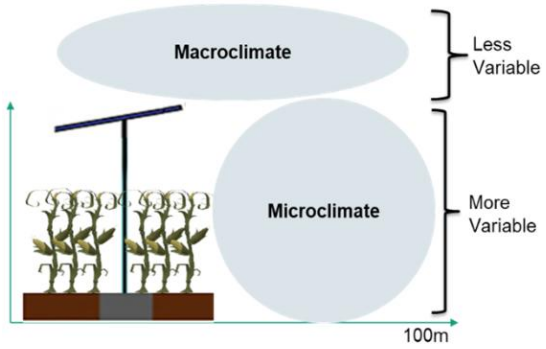

Figure 2.4: Illustration of a microclimate in an Agrivoltaic system [26]

Factors affecting the development of microclimates.

Various environmental factors play a significant role in the development of microclimates within agrivoltaic systems, such as humidity, soil moisture, wind speed, and evapotranspiration. The interaction of these factors beneath the partial shade of PV panels results in cooler and more humid conditions relative to open fields, which subsequently affects agricultural productivity and solar panel efficiency [15].

- **Moisture content in the air**

The presence of PV panels creates partial shading, which diminishes the direct sunlight exposure on the soil surface. This results in a decrease in soil temperatures and a reduction in the evaporation of soil water. The relative humidity beneath the panels is generally elevated compared to that in open fields [15].

- **Soil moisture**

The presence of shading from solar panels effectively reduces the rate at which soil water evaporates, leading to enhanced conservation of soil moisture levels. In areas where water resources are scarce, sustaining elevated soil moisture levels can significantly benefit crop development [16,27].

- **Velocity of Wind**

The installation of panels has the potential to decrease wind speeds at ground level by serving as a physical barrier. This interference with airflow results in the formation of a more stable air layer beneath the panels. The decrease in wind speed may yield varying impacts on crop growth [15].

- **Evapotranspiration**

Evapotranspiration is the process by which water is transferred from the land to the atmosphere through evaporation and transpiration. Research indicates that

evapotranspiration rates in agrivoltaic systems can be diminished by over 20% relative to open fields, influenced by factors such as climate, crop type, and the arrangement of solar panels [15]. Reduced evapotranspiration may lead to lower ambient temperatures, potentially enhancing the efficiency of PV modules by minimizing energy production losses associated with elevated temperatures.

Heat flux assessment in agrivoltaic microclimates

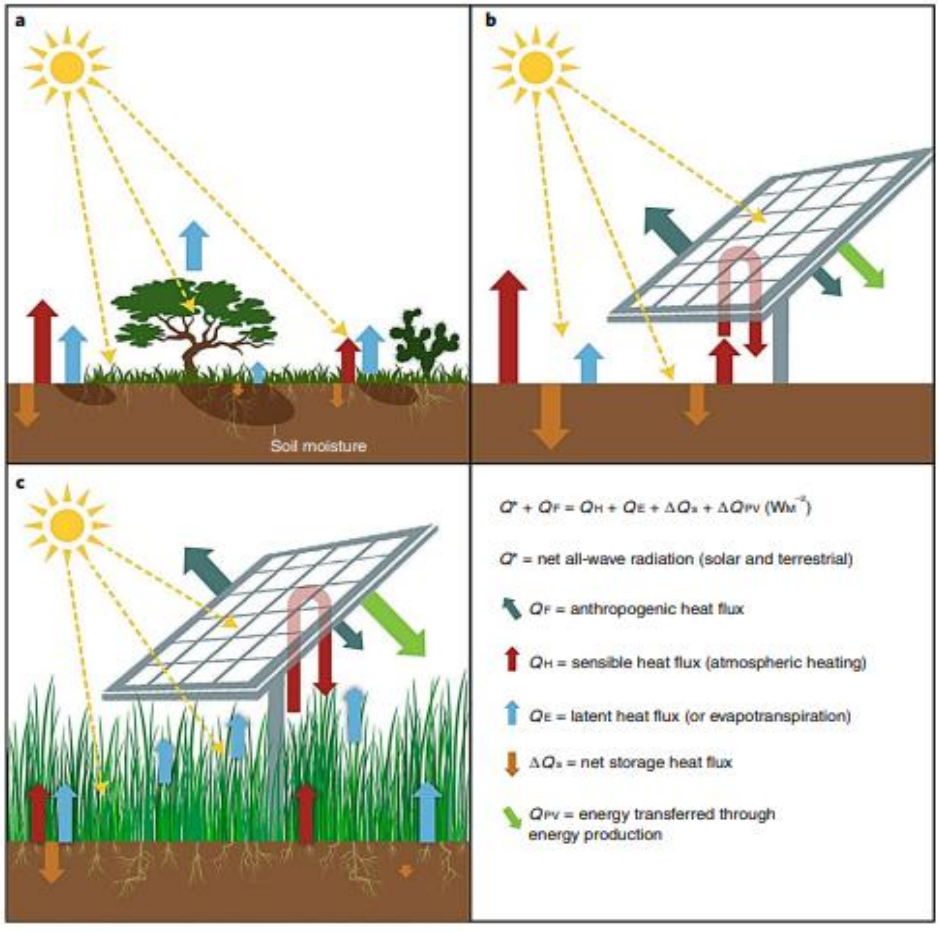

Figure 2.5: Changes in the exchange of heat fluxes with transition from a vegetated ecosystem (a), traditional PV installation (b) and finally to an Agrivoltaic system (c) [15].

Figure 2.5 compares the heat fluxes in a vegetated ecosystem and non-vegetated ecosystem (which are the majority of PV systems). Theoretically, the presence of vegetation under PV modules could potentially alter the exchange of the heat fluxes within the microclimate and contribute to a cooler module temperature [15]. Assuming identical rates of incoming solar energy (dashed yellow arrows), when a vegetated ecosystem (a) transitions to a solar PV installation (b), the energy flux dynamics of the area will be dramatically altered due to the loss of vegetation and the resulting latent heat fluxes (blue arrows). Increased fluxes of sensible heat (indicated by the red and orange arrows) result from transitioning to non-agrivoltaic systems, raising localised temperatures. The restoration of latent heat fluxes and sensible heat loss to the atmosphere are achieved by reintroducing vegetation (c), in this instance agricultural plants. Additionally displayed are the amounts of energy that PV panels convert to electricity (green arrows) and reradiate (teal arrows) and. The extent of each effect is correlated with the size and abundance of arrows [15].

Therefore, theoretically, it can be hypothesised that the microclimate in agrivoltaic systems provides cooler air temperature than air temperature between the ground and PV panels.

Summary of the microclimate findings:

The influence of crops on the panels was studied by Marrou et al. [16,17] and by Jung [27] who measured how the air temperature, wind speed, soil temperature, solar radiation, soil moisture and evapotranspiration change within the microclimate compared to a traditional agricultural setting.

Marrou et al. [16] found that neither the microclimate air temperature nor the wind speed was greatly influenced by the presence of crops which was in contrast with the findings of Trommsdorff et al. [12] and Barron et al. [15]. The contrasting findings can be attributed mainly to the design of the system, particularly the height of the PV modules. On the other hand, all the studies found significant reduction in water loss through evapotranspiration in the agrivoltaic system than in the normal agricultural control setting.

Similarly, a study by Kuleape et al. [26] modelled the heat fluxes and evapotranspiration within the microclimate and found that the soil temperature reduced by 17% while the evapotranspiration reduced by 10-15%. A significant number of these studies, except for Barron et al. [15], compared their findings to those of a typical agricultural system "control," but not always to those of a standard PV system. Consequently, it is necessary to evaluate how well PV modules function in an agrivoltaic setting in comparison to PV modules installed traditionally. This will give farmers and PV developers insights into what to anticipate in terms of energy yield from the modules when integrated into agricultural setting as opposed to a typical installation.

2.3. Examination of the challenges and limitations of Agrivoltaic systems: Technology and Finance

The potential benefits of agrivoltaic are evident; however, the adoption of this technology faces significant technological and financial barriers that complicate large-scale implementation. These challenges are such as:

- **High capital costs**

The initial investment required for agrivoltaic systems tends to exceed that of conventional solar or agricultural configurations. The increased expense is linked to the installation of elevated PV arrays, which need to be positioned at a height that permits crop growth and the operation of agricultural machinery while also ensuring adequate sunlight exposure for the crops [12].

A study conducted by Trommsdorff et al. [12] indicated that agrivoltaic systems may incur installation costs that are over 20% higher than those associated with standard ground-mounted solar installations. The presence of these additional costs could discourage potential adopters, particularly among small-scale farmers who have constrained financial resources. Thus, the profitability of these investments is contingent upon the integration of revenue generated from both agricultural products and electricity sales [28]. The fluctuations in crop prices and energy tariffs introduce additional complexities to the financial planning of agrivoltaic projects.

- **Design Considerations for Various Crop Categories**

Designing PV structures to support a diverse range of crops presents a multifaceted challenge, given that each crop possesses unique requirements for light, water, and space.

Crops that exhibit significant height, such as corn or sugarcane, necessitate greater panel elevations in contrast to shorter crops like lettuce or herbs. The differences in crop heights require adaptable designs that can be modified to accommodate various farming methods [23].

- **Examination of Policy and Regulatory Issues**

The absence of well-defined regulatory frameworks for dual-use land practices in various countries, impedes the implementation of agrivoltaic systems. In numerous areas, there is a lack of established policies concerning zoning regulations, land-use permits, and tax incentives relevant to agrivoltaic installations [12]. To facilitate the growth of agrivoltaic adoption, it is essential for governments to implement clear policies that promote dual-use practices and offer financial incentives to mitigate the elevated initial costs.

Chapter 3: Photovoltaic Technology

3.1. Fundamentals of photovoltaic energy transformation

The sun provides 99% of the energy on earth in the form of solar radiation [29]. However, due to atmospheric absorption and scattering, only a small percentage (<50%) reaches the earth surface [30]. Solar radiation is composed of tiny energy packets known as photons. The energy of these photons can be determined using Planck's law, expressed as:

$$E_{ph} = h \times v \qquad 3.1$$

Where E_{ph} is the energy of the photon, v is the frequency of light and h is Planck's constant.

The intensity of solar energy received at a specific area on the earth surface is known as the solar irradiance, expressed in watts per square meter (W/m^2). Solar irradiance is typically measured three ways, known as:

- Direct Normal Irradiance (DNI), which is the solar radiation received directly on a surface that is oriented perpendicular to the incoming rays.
- Diffuse Horizontal Irradiance (DHI), which refers to the amount of solar radiation received per unit area on a horizontal surface from the earth's atmosphere, excluding direct radiation.
- Global Horizontal Irradiance (GHI), defined as the total of Direct Normal Irradiance (DNI) and Diffuse Horizontal Irradiance (DHI) received on a horizontal surface.

The albedo effect

The albedo effect describes the amount of sunlight a surface (e.g. grass, crops etc.) is able to reflect back into the atmosphere. The albedo coefficient varies between 0, indicating a perfect absorber, and 1, representing a perfect reflector. In agrivoltaic systems, the albedo varies between 0.2 and 0.3, influenced by factors such as vegetation and soil moisture, which affects the overall energy captured by bifacial PV modules [31].

3.2. Photovoltaic effect

The process of generating electricity in a solar cell is based on the photovoltaic effect, which involves the direct conversion of light energy into electrical energy [32,33]. Photovoltaic panels are composed of numerous solar cells, which are fundamentally p-n junctions created by the combination of p-type and n-type semiconductor materials. In a p-n junction, the p-type material is formed by doping a semiconductor material e.g. silicon with elements from group III of the periodic table, which creates holes as positive charge carriers. On the other hand, the n-type material is formed by doping a semiconductor material e.g. silicon with elements from group IV of the periodic table, which creates electrons as negative charge carriers. This junction establishes an electric field at the interface, which is essential for charge separation [34].

When photons hit the solar cell, they can impart their energy to electrons in the valence band, enabling these electrons to transition to the conduction band if the energy of the photon is greater than or equal to the bandgap energy (E_g), of the cell. This process

generates electron-hole pairs. Electrons are excited into the conduction band while corresponding holes are left in the valence band. The electric field established at the p-n junction causes electrons to migrate towards the n-type region while holes move towards the p-type region, resulting in a potential difference across the junction [35]. When the cell interfaces with an external circuit, the separated charges migrate, producing an electric current that can be utilized for power generation.

The band gap energy of a solar cell is given by:

$$E_g = E_c - E_v \qquad 3.2$$

Where E_g is the bang gap energy, E_c is the conduction band energy and E_v is the valence band energy.

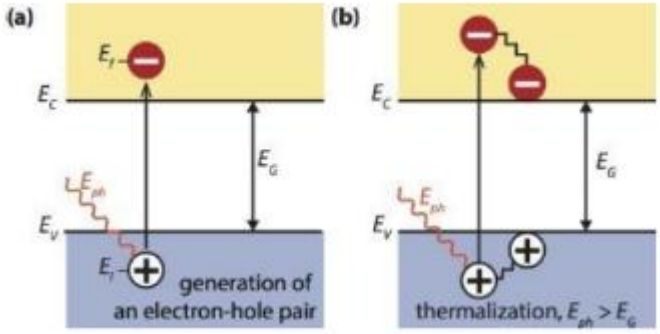

Figure 3.1: Illustration of the generation of an electron-hole pair when $E_{ph} = E_g$ (a). While (b) demonstrates thermalisation which happens when a photon with enrgy $E_{ph} > E_g$, excites an electron above the conduction band edge [36].

When an external circuit is connected to a solar cell, the potential difference generates an electric current, transforming absorbed light energy into usable electrical energy. The effectiveness of this process is determined by several factors, including the incident

photons' energy in relation to the band gap, doping levels, material quality, and cell design. Photons with energies less than the band gap do not generate electricity, but those with energies much higher than the band gap lose extra energy as heat. This process continues if light strikes the solar cell, allowing for the continued creation of electrical energy from sunlight [29].

3.3. Categories of PV Technologies

There are various types of PV technologies, including:

- **Monocrystalline Silicon Solar Cells**

Monocrystalline silicon cells exhibit a single, continuous crystal structure, contributing to their notable efficiency, which can surpass 22% in commercially available products [37]. The manufacturing process requires significant energy due to the necessity of growing single crystal ingots and subsequently slicing them into wafers. Monocrystalline cells incur higher costs in comparison to alternative types. Their high efficiency makes them appropriate for scenarios with spatial constraints, including rooftops and small-scale residential setups.

- **Polycrystalline Silicon Solar Cells**

On the other hand, polycrystalline cells consist of silicon crystals that have been fused through a melting process. The efficiencies typically fall within the range of 15-18%, primarily due to grain boundaries that obstruct electron flow [35]. The manufacturing

process for these cells is less energy-intensive, resulting in lower production costs compared to monocrystalline cells. Thus, this technology is most suitable for farms where space constraints are minimal, primarily because of their cost-effectiveness.

- **Thin-Film Solar Cells**

These cells utilize a minimal layer of semiconductor material, including cadmium telluride (CdTe) or copper indium gallium selenide (CIGS), which is applied onto a substrate. Efficiencies generally fall between 12-18%, yet recent innovations have brought certain thin-film technologies nearer to 20% [38]. Thin-film cells typically have lower manufacturing expenses due to their reduced semiconductor material requirements and the ability to utilize roll-to-roll manufacturing techniques. Their applications include large-scale implementations, building-integrated photovoltaics (BIPV), and portable solar products, attributed to their flexibility and lightweight characteristics.

- **Perovskite Solar Cells**

The crystal structure of perovskite cells, akin to that of calcium titanium oxide, enables efficiencies that exceed 29% when utilized in tandem configurations with silicon. The material exhibits a broad absorption spectrum and demonstrates significant potential for attaining efficiencies that surpass those of silicon [37]. Their notable advantage lies in the potential for cost-effective manufacturing, given that perovskites can be synthesized through solution-based processes. Nonetheless, concerns regarding long-term stability and toxicity, particularly related to lead content, require further attention. Therefore,

research is focused on the use of perovskites in tandem solar cells, where they are integrated with silicon to enhance overall efficiency, as well as in the development of flexible solar panels.

3.4. I-V curve of a solar cell

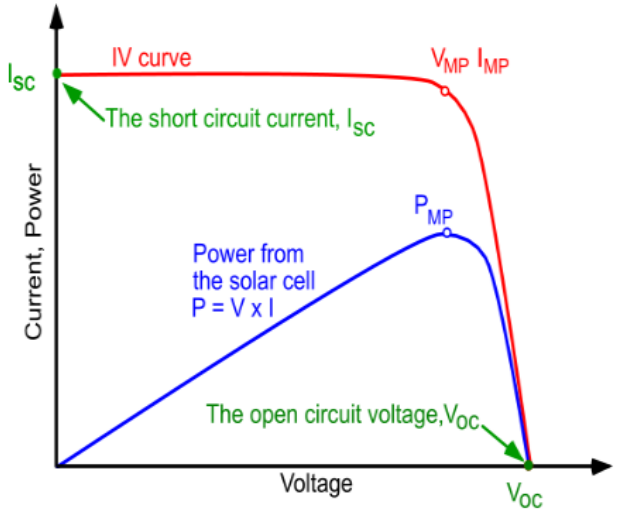

Figure 3.2: I-V characteristic of a solar cell [29]

Figure 3.2 illustrates an I-V curve, which is a graphical representation of the relationship between the total output current, *I* and the output voltage, *V* of a solar cell. The I-V curve of a solar cell describes the performance of a solar cell under varying operating conditions. To plot the I-V curve of a solar cell, the load voltage, *V* is varied from zero to a maximum value, and at each voltage point a corresponding external output current, *I* is obtained [33].

Some of the important points on an I-V curve under any operation conditions are short circuit current, I_{sc}, open circuit voltage, V_{oc} and Maximum Power Point, MPP or P_{MP} as labelled on the curve.

The I_{sc} is the maximum output current obtained from the solar cell when the voltage is zero (short circuit condition). It indicates the maximum current a cell can generate under illumination. The short circuit current significantly depends on the area of the solar cell, solar irradiance and the properties of the solar cell material. While V_{oc} is the maximum output current and is obtained when the current is zero (open circuit condition). It indicates the maximum voltage that can result across the cell under illumination. The V_{oc} depends on the quality of the material, specifically the value of the dark saturation current, I_o. The lower the value of I_o, the higher the quality of the material and therefore the higher the V_{oc}. Lastly, MPP, is a point on the I-V curve where the product of current and voltage is maximum [29].

The values of the I_{sc}, V_{oc} and MPP are specified by the manufacturers at standard test conditions (STC) and written on the data sheet. The standard test is done at $1000\ W/m^2$ normal irradiance, $25℃$ cell temperature and air mass 1.5 solar spectrum.

Another performance parameter of a solar cell or module is the fill factor, which is a ratio of the maximum power (P_{mpp}) to the product of the open circuit voltage and short circuit current. It indicates how closely the operating voltage and current of cell approach the theoretical maximum. A good quality module typically has a fill factor above 0.75, signifying more efficient power extraction.

3.5. Impact of climate condition on the IV curve

Climatic conditions have a significant effect on the performance of a solar module. These influences are typically depicted on the I-V curve. The main environmental conditions are temperature and solar radiation intensity.

3.5.1. Effect of temperature

The temperature of a solar cell depends on the ambient temperature, the intensity of the incident light and the heat exchange capabilities of the cell material. The ambient temperature is also one of the major environmental factors that influence the operating temperature and the performance of solar modules. The effect of the operating temperature is shown in Figure 3.3. The I-V curve was plotted for a 255 W solar panel with 60 solar cells in series at a constant irradiance of $1000\ W/m^2$ and an air mass of 1.5 at different operating temperatures. The temperature is varied between 5 ℃ - 65℃ and the corresponding I-V characteristic is plotted.

As the temperature of the panel increases, the bandgap decreases which results in a larger part of the spectrum to be absorbed. This causes a slight increase in the short circuit current I_{sc}. The slight increase in I_{sc}. with temperature is also due to the enhancement of thermal generation of charge carriers. As depicted by the curves in Figure 3.3, increasing the temperature of a solar module decreases the V_{oc} dramatically. This is because at high temperatures the concentration of intrinsic charge carriers of a semiconductor increases which results in high recombination rates and a decrease in V_{oc} [39]. A decrease in V_{oc} is also mainly due to an increase in I_o which increases with temperature [29,33].

Overall, an increase in I_{sc} is relatively small compared to a decrease in V_{oc}, therefore the maximum power output of the panel decreases as the temperature increase.

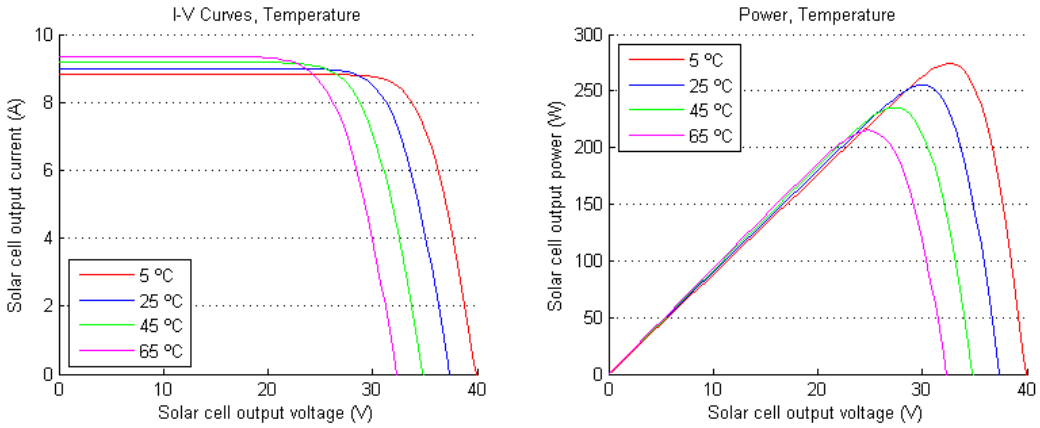

Figure 3.3: Illustration of the I-V and Power curves under varying temperature [40]

3.5.2. Effect of solar irradiance

Figure 3.4Figure 3.4 illustrates the I-V curve of a 255 W solar panel with 60 cells in series at a constant operating temperature of 25 °C and air mass of 1.5 with a variation in the irradiance levels. The irradiance is varied between 400 W/m^2 and 1000 W/m^2 and the corresponding I-V curve is plotted. The effect of temperature on the power curve is also shown on the right-hand curve [40].

As it can be seen in Figure 3.4, current decreases significantly with a decrease in solar radiation. Short circuit current, I_{sc} varies linearly with the level of irradiance. This is because as solar radiation increases, the number of photons hitting the solar panel also

increases, resulting in the generation of more charge carriers and thus increasing the current [33].

On the other hand, the open circuit voltage increases logarithmically with an increase in irradiance, however the effect is very minimal and can be neglected in most cases [33]. In summary, high solar radiation results in increased current and negligible rise in voltage which consequently results in increased output power of the solar panel.

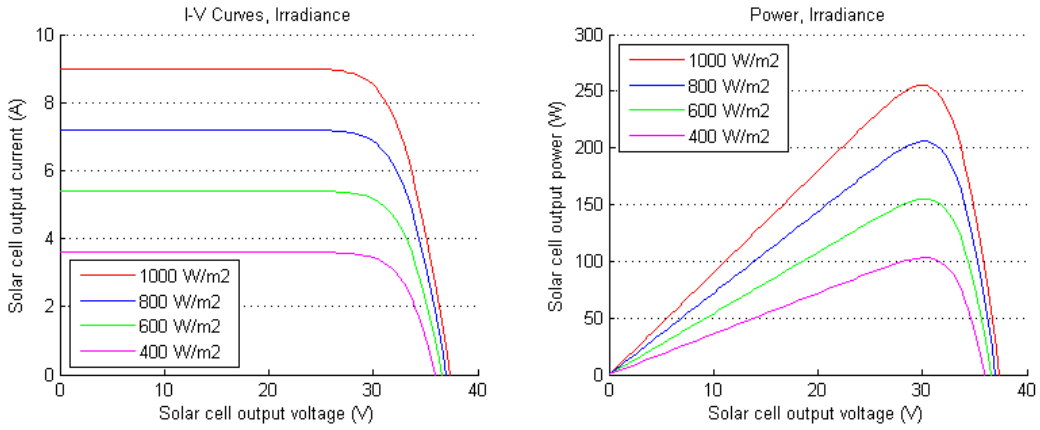

Figure 3.4:Illustration of the I-V and Power curves under varying solar irradiance [40]

3.6. Causes and impacts of the heating effect in PV modules

The heating effect of PV modules remains a huge concern despite technological advancement in PV systems [41]. Research continues to explore ways to mitigate this important concern. There are several factors that causes PV module to heat up during operation [42,43].

The primary contributor is the inability of PV modules to absorb all the incident radiation regardless of its spectral properties. Only about 20% of incident light is converted to

electricity in a PV module and part of the remaining 80% may be dissipated as heat raising the temperature of the module [44]. Other causes may include very hot weather conditions, high packing density of solar cells within a module and the properties of the module materials [29].

High temperatures have detrimental impacts on the performance and degradation rate of PV modules. PV modules have a negative temperature power coefficient of about 0.5%/℃. This means its power decreases by about 0.5% for each degree Celsius above the standard temperature of 25℃. Higher temperatures reduce the power output and efficiency of PV modules [44].

Additionally, long-term exposure to high temperatures can result in accelerated degradation, thermal stress and cracking, hot spots, increased resistance, and safety concerns. Therefore, it is crucial to mitigate this effect [44].

3.7. Methods for reducing PV temperature

There are various methods of cooling PV panels, which can be categorised as either passive cooling or active cooling. Passive cooling are cooling methods that do not require additional mechanical equipment and external sources for cooling [45]. This method uses evaporation, natural convection, radiation to dissipate stored heat from the panel [46–49]. Passive cooling mechanisms are typically less costly. Active cooling, on the other hand, involves mechanisms that involve the design modification of the solar cells or modules [50]. It may also include the incorporation external source of energy and additional

mechanical equipment to circulate the cooling medium. Active cooling methods are relatively more effective, but they are also more costly.

3.7.1. Passive cooling methods

The methods of passive cooling include:

- **Tilted Panel Configurations**

Here the angle of the PV panels is adjusted to an optimal position to facilitate natural convection, which effectively cools the surface of the module. The tilt angle is adjusted according to geographic location and seasonal variations, optimizing airflow beneath the panel and minimizing heat accumulation [51].

- **Ventilated Photovoltaic Installations**

Ventilated designs consist of the installation of PV modules with a space between the module and the mounting surface, such as a rooftop, which facilitates unobstructed airflow beneath the panel. The natural airflow facilitates a more efficient heat dissipation compared to panels that are mounted directly [45].

- **Materials and Coatings that Reflect**

This involves the application of reflective materials or coatings to the surface of PV modules can decrease the heat absorption by reflecting a portion of the sunlight away from the module [45].

3.7.2. Active cooling methods

- **Water Application**

Water spraying is a method that consists of periodically applying water to the surface of photovoltaic modules to facilitate heat removal. This method demonstrates notable effectiveness in regions characterized by high ambient temperatures and limited water availability, particularly in hot and arid climates [52].

Phase Change Materials (PCMs)

PCMs function by absorbing surplus heat through a phase change, such as transitioning from solid to liquid, at designated temperatures. The integration of these components into the back of the PV modules facilitates the absorption and storage of thermal energy throughout the day, followed by its release during periods of temperature decline [52].

Forced air cooling

Forced air cooling employs fans or blowers to move air over the surface of the PV modules, thereby improving convective heat transfer. This approach proves to be especially effective for extensive solar farms, where natural convection alone may fail to ensure optimal temperature regulation [42].

Chapter 4: Models for predicting module temperature

Studies have indicated that it is challenging to find one model that describes the module operating temperature for all PV modules installed in different climatic conditions and installation methods. For example, the temperature coefficients for PV modules installed via the ground-mounted method (non-agrivoltaic) will be different from those PV modules installed in an agrivoltaic method (for example). This is due to differences in heat exchange mechanisms. Similarly, the heat exchange mechanisms for a PV system in arid climate will be different to a system in a humid climate condition. Therefore, there are various models employed to predict the operating temperatures of PV panels in various climatic conditions and installation types.

These models range in complexity from simplified equations with few variables to complex 3-dimensional computational fluid dynamics (CFD) simulations that account for heat exchange across module layers and interactions with the environment. The complex models consider both dynamic and steady-state energy balances, which are influenced by climatic variables like wind and irradiance. However, due to the challenge of acquiring extensive data and the computing complexity involved, existing models often make simpler assumptions. Comparative studies such as [53,54] , which have mostly focused on ground-based systems, have carefully analysed these models, highlighting their reliance on elements such as incident irradiance, ambient temperature and, in some cases, wind speed to improve precision.

Therefore, this section reviews common module temperature prediction models and identify their reliance on different input parameters.

4.1. Faiman Model

The Faiman model is based on basic principles of heat transfer principles to predict the temperature for outdoor PV modules as detailed in [55]. It uses the heat loss coefficients U_0 and U_1 to simplify the complex thermal dynamics within a PV module. The coefficient U_0 is related to heat losses from radiation and convection, while U_0 is related to convective heat transfer due to wind. The model has gained wide acceptance in the PV industry and has been integrated into the IEC 61853 standard. This model is also adopted for use in the leading PV simulation software such as PVsyst.

The Faiman model is expressed as:

$$T_{mod} = T_{amb} + \frac{G_T}{U_0 + U_1 * WS} \quad 4.1$$

Where:

- T_{mod} – module temperature (℃)
- T_{amb} – ambient temperature (℃)
- G_T – solar irradiance on the solar module (POA) ($\mathrm{W/m^2}$)
- WS – wind speed (m/s)
- U_0 is the heat-loss coefficient due to natural heat exchange ($\mathrm{W/m^2℃}$).
- U_1 is the convective heat-loss coefficient due to the influence of the wind (W/m^2℃).

The parameters of U_0 and U_1 are tuned or fit based on experimental data. The default values for an open rack installation in a desert condition are $U_0 = 25\ W/m^2°C$ and $U_1 = 6.84\ W/m^2°C$.

The Faiman model relies on the solar irradiance incident on the panel, ambient temperature, wind speed and site-specific coefficients, which makes the module simple and yet effective. By adjusting the coefficients to local conditions, the model is adaptable across diverse climates. Faiman model is widely used mainly due to its adaptability even in the absence of precise heat transfer data.

Although the model is effective for fundamental applications, it does not sufficiently account for all heat transfer complexities such as infrared radiative losses, which could result in an underestimation or overestimation in extreme climates. Nevertheless, the accuracy of the model can be optimised by fine-tuning the U_0 and U_1 through field data calibration.

4.2. Sandia Model

The Sandia model is a more complex temperature prediction model that incorporates various environmental factors such as mounting configuration, air mass, module tilt and wind cooling effects in more detail. This model requires extensive computational approach and module-specific details to compute the dimensionless coefficients a and b.

The Sandia model is expressed as:

$$T_{mod} = T_{amb} + G_T * e^{a+b*WS} \qquad 4.2$$

Where:

- T_{mod} – module temperature (°C)
- T_{amb} – ambient temperature (°C)
- G_T – solar irradiance on the solar module (POA) (W/m^2)
- a describes the radiation effect on the module.
- b describes the cooling effect due to wind influence.

The model is developed by the Sandia National Laboratories as detailed in [56] and has been validated using multiple field data points, which makes it appropriate for high precision applications. Sandia model has also gained significant acceptance within the PV industry due to its high accuracy for specific installations attributable to its comprehensive consideration of environmental parameters.

The necessity for detailed inputs results in the process to be data-intensive, posing constraints when certain parameters, such as module configuration or incident angle are not readily accessible. Due to the constraints of standard field data in this study, the usage of the complex Sandia model for this study would be impractical.

4.3. Zenit Model

Zenit model is a Python package for PV system simulation developed by the Fraunhofer ISE [57]. It is designed for annual average simulations and comes with yield evaluation tools. Zenit provides a comprehensive and extremely flexible simulation suite, but it places a higher priority on speed than accuracy [54].

Zenit model is given by:

$$T_{mod} = T_{amb} + T_s \times \frac{G_T}{1000} \quad 4.3$$

Where:

- T_{mod} – module temperature (℃)
- T_{amb} – ambient temperature (℃)
- G_T – solar irradiance on the solar module (POA) (W/m^2)
- T_s represents the influence environmental factors such as wind. It is independent of the PV technology, but it depends on the mounting methods such as integrated PV and ground-mounted PV.

4.4. Standard Model (Nominal Operating Cell Temperature (NOCT)

NOCT is a standard for predicting the operating temperature of solar cells under the following standard conditions: ambient temperature of 20 ℃, irradiance of 800 W/m^2, wind speed of 1 m/s [54]. This method is commonly employed for preliminary feasibility evaluations. It is simple to implement, offering a general estimation of module temperature and facilitating basic performance predictions in absence of detailed environmental data.

The model exhibits limitations in its adaptability to varying weather patterns and site-specific predictions.

NOCT is given by:

$$T_{mod} = T_{amb} + \frac{G_T}{G_{NOCT}} * (T_{NOCT} - T_{amb.NOCT}) \quad 4.4$$

Where:

- T_{mod} – module temperature (℃)
- T_{amb} – ambient temperature (℃)
- G_T – solar irradiance on the solar module (POA) (W/m^2)
- G_{NOCT} is the irradiance at NOCT condition (800 W/m^2)
- T_{NOCT} is the cell temperature at NOCT (℃)
- $T_{amb.NOCT}$ is the ambient temperature at NOCT (℃)

4.5. PVsyst Model

The PVsyst temperature prediction model is widely used in the PVsyst software to estimate the cell temperature of PV modules by using an empirical heat loss factor model [58]. The model is fundamentally based on the Faiman model, and it is widely accepted in the PV industry, making it suitable for feasibility studies and general performance estimates. It integrates effectively with commercial simulation software, enhancing user-friendliness for project planning. The values of the coefficients U_c and U_v are dependent on the module technology and installation methodology. For a typical ground-mounted PV systems the values are typically; $U_c = 29.0\ W/m^2$℃ and $U_v = 0.0\ \mathrm{W/m^2}$℃.

The PVsyst model is expressed as:

$$T_{mod} = T_{amb} + \frac{G_T * (1 - \eta_m)}{U_c + U_v * WS} \quad 4.5$$

Where:

- T_{mod} – module temperature (℃)
- T_{amb} – ambient temperature (℃)
- G_T – solar irradiance on the solar module (POA) ($\mathrm{W/m^2}$)
- WS – wind speed (m/s)
- U_c represents the effect of radiation on the module temperature ($\mathrm{W/m^2℃}$).
- U_v represents the convective heat transfer ($\mathrm{W/m^2℃}$).
- η_{m} represents the efficiency of the module.

However, the reliance of PVsyst on generalised NOCT assumptions constraints its accuracy, as NOCT is not well-suited to varying climates. Thus, the generalised approach of PVsyst could introduce inaccuracies due to specific environmental factors involved in this study.

4.6. Skoplaki Model 1

Skoplaki developed two separate models, which were considered. The models emphasize convective and radiative heat losses through a simplified expression that incorporates ambient temperature, irradiance, and convective losses [59]. The first model, here as 1, is simpler and does not account for specific factors that are dependent on the PV module, resulting in temperature predictions that are independent of the PV technology and mounting style.

This model is given by:

$$T_{mod} = T_{amb} + \frac{0.32}{8.91 + 2.0 * WS} * G_T \quad 4.6$$

Where:

- T_{mod} – module temperature (℃)
- T_{amb} – ambient temperature (℃)
- G_T – solar irradiance on the solar module (POA) (W/m^2)
- WS – wind speed (m/s)

4.7. Skoplaki 2 Model

The second Skoplaki model is more complex and considers module specific parameters such as temperature coefficient of the maximum power and efficiency [60], as it extends the first Skoplaki model by incorporating supplementary factors associated with radiative cooling.

This model is expressed as:

$$T_{mod} = T_{amb} + \frac{G_T}{800} * (T_{NOCT} - 20) * \frac{h_{w.NOCT}}{h_w} * (1 - \frac{\mu_{STC}}{0.9} * (1 - \beta_{STC} - T_{STC})) \quad 4.7$$

Where:

- T_{NOCT} is the nominal operating cell temperature
- h_w is the heat transfer coefficient due to wind calculated as: $h_w = 5.7 + 2.8 * \mathrm{WS}$
- $h_{w.NOCT}$ is obtained using the wind speed at NOCT conditions
- μ_{STC} is the efficiency of the module at STC conditions

- β_{STC} is the temperature coefficient of maximum power at STC
- T_{STC} is the temperature at STC condition (℃)

The Skoplaki models yield accurate temperature predictions for ground-mounted systems in standard conditions and are esteemed in academic research for their moderate data requirements. However, these models rely on specific constants for radiative and convective losses, which may not be applicable across varying climatic conditions. The absence of comprehensive heat transfer data in this study deems the application of Skoplaki models possibly challenging, as their simplifications may lead to inaccurate predictions.

Chapter 5: Research Methodology

5.1. Data acquisition and preparation

To accurately assess the thermal performance of photovoltaic modules in agrivoltaic (APV) systems, it is necessary to have both an APV test site and a typical non-APV control site. Non-APV systems in this context are PV modules installed in the standard configuration, without any crops beneath them. Both systems should ideally be situated within the same geographical region to guarantee equivalent exposure to climate variables, including sun irradiance, temperature, humidity, and wind speed.

The data for this study was gathered from two agrivoltaic sites, one of which is situated in Benin and the other in Büren, Germany. Nevertheless, neither site was equipped with an adjacent non-APV system that could serve as a direct control. In order to overcome this limitation, the meteorological data from the Benin APV site were utilized to model and predict the expected thermal performance of a similar non-APV system within the same region.

On the other hand, the data from Büren APV was used to fine-tune the heat transfer coefficients in Faiman's model to ensure that it accurately reflects the microclimate conditions unique to APV systems. Similarly, the data from Benin APV was also used to fine-tune the heat transfer coefficients to ensure accurate reflection of both the climatic and APV conditions in Benin. The fine-tuned coefficients were then independently applied to the Faiman model using similar Benin dataset to predict the thermal behaviour of the APV system in Benin. The detailed procedure is outline in this section.

Description of the Agrivoltaic project sites:

Benin Agrivoltaic site:

The site is known as the Agrivoltaic Songhai project, located in the southern area of Benin in West Africa at coordinates (6.499490°N, 2.61477°E) [61]. This site was selected because, during the study period, it was the only research project in Africa that provided a complete dataset for an entire crop season, suitable for analysis and that whose dataset was accessible for the study. A network of six Temperature & Moisture Sensors (TMSs) was utilized to collect data, with the sensors positioned randomly throughout the site. The site included two separate APV systems, with each system having an installed capacity of 15 kWp. Figure 5.1 illustrates that one system employed a strip layout, whereas the other utilized a checkerboard pattern. Each system contained three TMS sensors, which were distributed randomly throughout the designated area.

The APV systems cultivated mixed crops, with a focus on vegetables like peppers and onions. The sensors recorded multiple parameters, such as soil temperature, soil moisture, and ambient temperature, at three distinct layers. This study concentrated on ambient temperature data, which was recorded every 10 minutes over a period of 83 days, from April 21 to July 14, 2023, covering an entire crop season.

Figure 5.1: Benin Agrivoltaic systems: checkboard (left) and strip setup (right) [© Songhai]

Meteorological data from Solar-GIS for control purposes

The meteorological data, on the other hand, was sourced from the Solar Geographical Information System (Solar-GIS) database. Solar-GIS supplied meteorological data, including ambient temperature, solar radiation, wind speed, and soil moisture, at hourly intervals. The geographical coordinates of the Songhai Agrivoltaic project site were utilized to acquire the meteorological data set from Solar GIS. The data were utilized to hypothetically forecast the module temperature for PV modules in a non-Agrivoltaic setting, serving as a control data set.

Germany Agrivoltaic site

A dataset was acquired from an Agrivoltaic system in Germany, specifically the Büren Agrivoltaic, situated in Büren at the coordinates 51.586626°N, 8.543833°E. This Agrivoltaic system cultivates raspberries, as illustrated in Figure 5.2. The parameters of interest measured for this system include the microclimate ambient temperature beneath

the modules, microclimate wind speed, plane of array (POA) irradiance, and the module temperature.

Figure 5.2: Illustration of the Büren agrivoltaic system [© Fraunhofer ISE]

5.2. Procedure

The overview of the procedure for this study is presented in the flowchart in Figure 5.3, with the following steps outlined to ensure a clear methodological approach. The detailed modelling procedure is elaborated in detail in chapter Chapter 6:.

1. **Initial estimation of the module temperature:**

The initial estimation of module temperature was conducted utilizing the Faiman model along with the standard heat transfer coefficients: $U_0 = 25\ W/m^2°C$ and $U_1 = 6.84\ W/m^2$. The model was implemented independently for the Benin APV system and

a theoretical non-APV system used for comparison. Microclimate ambient temperatures were utilized for the APV modules, whereas meteorological ambient temperatures were applied for the non-APV system. Both estimations were based on data obtained from the Benin APV site.

2. Fine tuning the heat transfer coefficients

To enhance the model's precision, the heat transfer coefficients were refined using the Quasi-Newton optimization method, employing measured data from the Benin and Büren APV sites. Following the estimation of the initial module temperature for the Benin APV, a subsequent adjustment of the Faiman model coefficients was performed utilizing microclimate data from an alternative temperature sensor located within the Benin APV site. This step was intended to enhance the model for both APV conditions and the unique climatic conditions present in Benin, which are not entirely addressed by the standard Faiman coefficients.

In a similar manner, the Büren APV dataset was utilized for further fine-tuning of the Faiman coefficients. The Büren dataset, in contrast to the Benin dataset, incorporated direct measurements of module temperature. The refinement using Büren data was instrumental in ensuring that the model effectively captured APV microclimates, as it had access to measured module temperatures, unlike in Benin, where module temperatures were only predicted.

3. Final PV module temperature calculation

The final temperature of the PV module was calculated for both APV and non-APV conditions using the newly fine-tuned coefficients, applying the Faiman model. This step

included the modified coefficients from both the Benin and Büren sites, enhancing the model to align with the specific microclimate characteristics of APV.

4. Model accuracy assessment

The evaluation of the accuracy of the module temperature predictions involved a comparison of results obtained from three distinct sets of heat transfer coefficients—standard Faiman, Benin-tuned, and Büren-tuned—utilizing the Benin dataset as the input for analysis. Four metrics were utilized to evaluate the performance of the model: R-squared, Mean Squared Error (MSE), Mean Absolute Error (MAE), and Root Mean Squared Error (RMSE). This analysis offered a clear understanding of how effectively each coefficient set models PV module temperatures in the specific conditions of the Benin APV site.

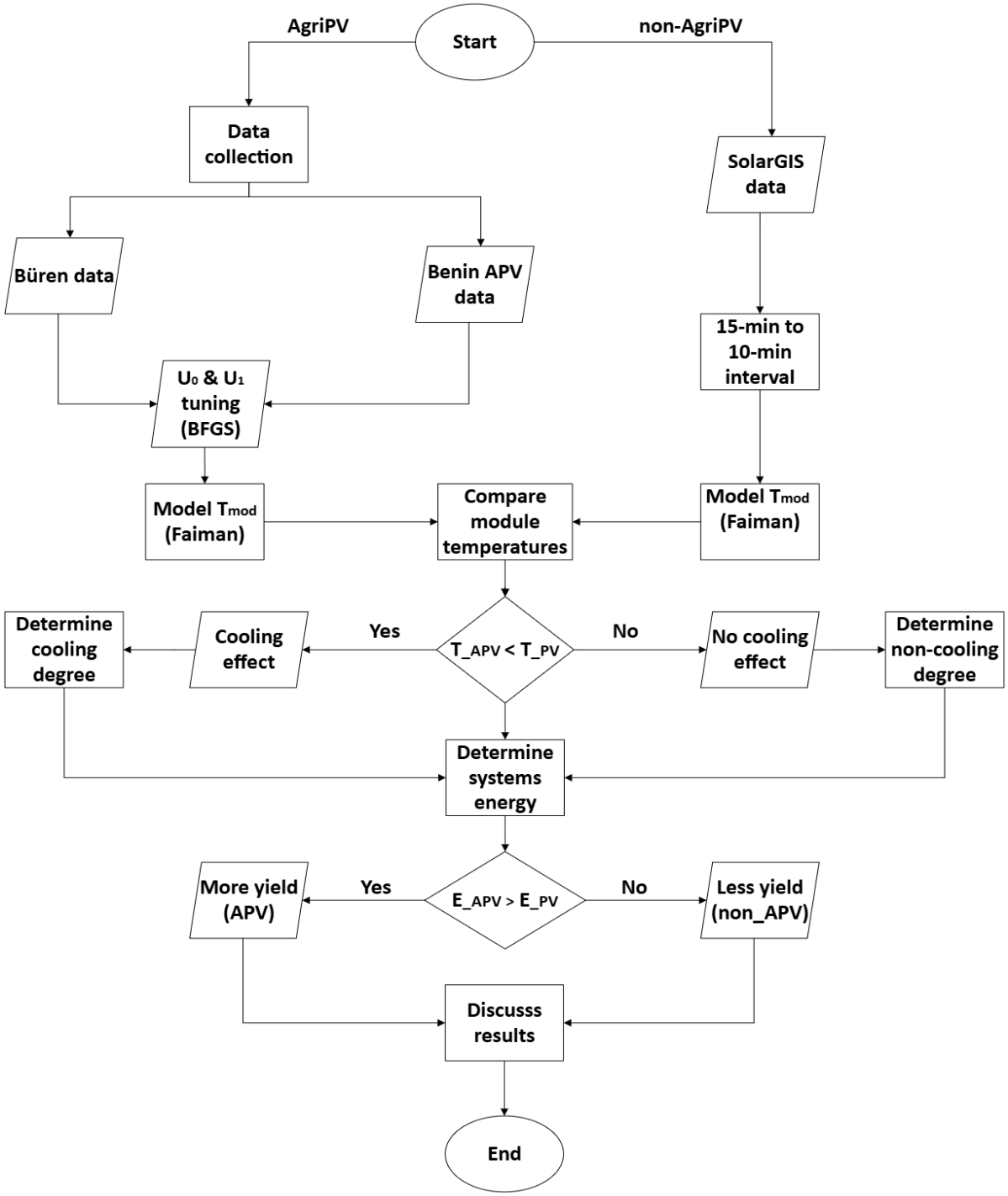

Figure 5.3: Flow chart of the methodological steps.

Chapter 6: Modelling of PV panel temperature and tuning heat transfer coefficients

6.1. Estimating module temperature for Benin agrivoltaic system using the standard Faiman heat transfer coefficients

To estimate the temperature of PV modules in the Benin agrivoltaic system, the Faiman model (Equation 4.1) was used, applying initial standard Faiman values for the heat transfer coefficients $\mathrm{U_0 = 25\ W/m^2{}^\circ C}$ and $\mathrm{U_1 = 6.84\ W/m^2}$. The model can be expressed as follows:

$$T_{mod} = T_{amb} + \frac{G_T}{U_0 + U_1 * WS}$$

Where:

- T_{amb} is the ambient temperature
- G_T is the irradiance on the plane of array (POA)
- WS is the wind speed

Ambient temperature (T_{amb}) was measured using ground-mounted sensors that were placed randomly throughout the agrivoltaic site. Conversely, the solar irradiance on the module surface (G_T)) and wind speed (WS) were obtained from the Solar GIS dataset. The model assumes that G_T is POA irradiance; however, the Solar GIS dataset provides irradiance in the forms of Direct Normal Irradiance (DNI), Diffuse Horizontal Irradiance (DHI), and Global Horizontal Irradiance (GHI). Therefore, the POA irradiance for the

modules, positioned at a tilt of 7° (which corresponds to the latitude of Benin), was determined by utilizing the DNI, DHI, and GHI values.

The wind speed data obtained from Solar GIS were measured at a standard height of 10 meters. To modify this to the module height of 2 meters, the wind profile power law was utilized (Equation 6.1), facilitating a more precise depiction of wind conditions at the module level [62]:

$$\boldsymbol{WS_2 = WS_1 \frac{\ln(\frac{h_2}{z_0})}{\ln(\frac{h_1}{z_0})}} \quad 6.1$$

Where:

- WS_2 is the adjusted wind speed at the module height h_2= 2 m
- WS_1 is the wind speed at the reference height h_1= 10 m
- z_0 is the roughness length, as outlined in Table 6.1.

The logarithmic wind profile offers a precise estimation of how vertical wind speed varies, particularly in flat terrain with neutral air stratification, by modifying the wind speed data from a 10 m reference height to correspond with the position of the PV module.

Table 6.1: Roughness classes and lengths [62]

Roughness class	**Roughness length z_0**	**Types of land cover**
0	0.0002 m	Surfaces of water e.g. lakes and seas
0.5	0.0024 m	Open terrain with a smooth surface, e.g. mown grass, airport runways, concrete etc.
1	0.03 m	Open agricultural land without hedges and fences
1.5	0.055 m	Agricultural land with a few buildings and 8 m high hedges with a separation of more than 1 km
2	0.1 m	Agricultural land with a few buildings and 8 m high hedges with a separation of about 500m
2.5	0.2 m	Agricultural land with many plants, trees, and bushes
3	0.4 m	Villages, small towns, agricultural land with forests, many or high hedges and uneven terrain
3.5	0.3 m	Big towns with high buildings
4	1.6 m	Big cities with high skyscrapers and tall buildings.

6.2. Estimating module temperature for Benin non-Agrivoltaic system using the standard Faiman heat transfer coefficients

The exact same method was utilized to calculate the anticipated temperature of a PV module in an anticipated non-agrivoltaic system at the Benin site. In this non-APV system, the ambient temperature input was obtained directly from meteorological data supplied by Solar GIS, as opposed to the microclimate measurements utilized for the agrivoltaic system. Therefore, the sole distinction in the calculation of module temperature between the two systems was the source of ambient temperature. All other factors, such as the plane of array (POA) irradiance, wind speed, and the standard Faiman heat transfer coefficients, were consistent in both models. The following plots were obtained.

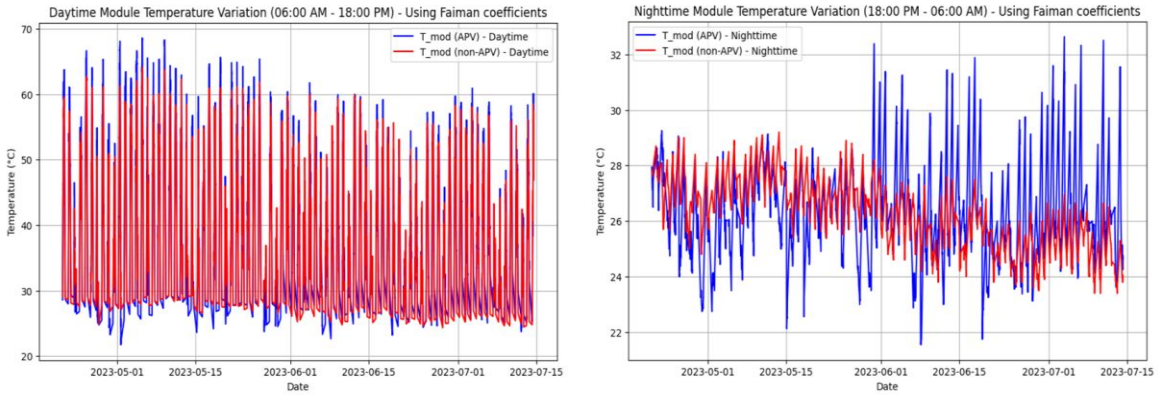

Figure 6.1:Daytime and nighttime module temperature variation over time using the standard Faiman heat transfer coefficients ($U_0 = 25\ W/m^2$℃ *and* $U_1 = 6.84\ W/m^2$℃ *). The blue plots represent the agrivoltaic module temperature values while the red plots are for the non-agrivoltaic module temperature values.*

6.3. Tuning Benin heat transfer coefficient from Benin Agrivoltaic dataset

After estimating the PV module temperature for the Benin agrivoltaic system using the initial standard heat transfer coefficients in the Faiman model, data from an additional sensor within the same system was utilized to refine the model, resulting in a new Benin-specific coefficient for enhanced accuracy.

The Broyden-Fletcher-Goldfarb-Shanno (BFGS) algorithm [63], which is a Quasi-Newton optimization method, was used to adjust these site-specific coefficients. This optimization algorithm reduces the discrepancy between actual and predicted temperatures through a process of iterative adjustment of the coefficients. The process is carried out using an objective function, as illustrated in Equation 6.2, which seeks to minimize the residual error, specifically the mean squared error (MSE), between the observed and predicted temperature values.

The BFGS algorithm starts with initial coefficient estimates that serve as the basis for calculating predicted module temperatures. The process involves iteratively updating the coefficients to achieve convergence through the continuous minimization of the MSE. As a result of the optimization process, the site-specific Benin coefficients were established as: $U_0 = 24.4\ \mathrm{W/m^2{}^\circ C}$ and $U_1 = 11.8\ \mathrm{W/m^2{}^\circ C}$, which provides a more precise representation of the heat transfer dynamics in the context of Benin's agrivoltaic conditions.

$$Objective\ Function: f(U_0, U_1) = \sum_{i=1}^{n} \left(T_{mod,actual,i} - T_{mod,predicted,i}\right)^2 \quad 6.2$$

Where:

- $T_{mod,actual,i}$ is the actual measured module temperature value of the i[th] data point
- $T_{mod,predicted,i}$ is the predicted value of the i[th] data point.

6.4. Tuning Büren heat transfer coefficient from Buren Agrivoltaic dataset

The dataset obtained from the Büren agrivoltaic facility was utilised to calibrate the heat transfer coefficients for the Faiman model. The Büren dataset, in contrast to the Benin agrivoltaic dataset, provided direct measurements of module temperature, which facilitated a more accurate calibration of the heat transfer coefficients. The calibration was crucial for developing coefficients that could be utilised to predict module temperatures in the Benin agrivoltaic system through a consistent methodology. After completing the calibration process, the heat transfer coefficients specific to Büren were found to be $U_0 = 35.8\ \mathrm{W/m^2°C}$ and $U_1 = 3.9\ \mathrm{W/m^2°C}$, which allows for precise predictions of module temperatures in Benin when utilised within the Faiman model.

6.5. Evaluation metrics for the performance of the three sets of heat transfer coefficient

The three sets of heat transfer coefficients; Faiman's standard coefficients, the Benin-tuned coefficients, and the Büren-tuned coefficients, were applied independently to the Faiman model to estimate PV module temperatures based on the Benin dataset. The module temperature estimates derived from each set of coefficients were subsequently

assessed using various quantitative metrics to evaluate model fit and facilitate comparison among the different coefficient sets. The evaluation metrics offer a clear understanding of the accuracy and predictive performance associated with each coefficient configuration. The metrics that have been applied are as follows:

- **The R-squared (R^2) value:** It is also known as the coefficient of determination, is a statistical measure that indicate how well the predicted values of the regression model fit the actual data. It ranges between 0 and 1. A value of 0 indicates a poor fit revealing that the model does not explain any variability in the data. While a value of 1 indicates a perfect fit showing that the model fully explains all the variability in the data [64].

$$R^2 = 1 - \frac{\sum_{i=1}^{n}(y_i - \hat{y}_i)^2}{\sum_{i=1}^{n}(y_i - \bar{y})^2} \quad 6.3$$

- **Mean Squared Error (MSE):** This metric measures the average squared difference between the actual and the predicted values. It is computed by averaging the squared the squared errors, or the variations between the values that had been and the actual values. A model that fits the data better is indicated by a lower MSE [64].

$$MSE = \frac{1}{n}\left(\sum_{i=1}^{n}(y_1 - \hat{y}_i)^2\right) \quad 6.4$$

- **Mean Absolute error (MAE):** This measure signifies the mean of the absolute discrepancies between expected and actual values. In contrast to MSE, its does not

square the errors, thus offering a more direct assessment of the inaccuracy. It is frequently more interpretable as it reveals the average size of errors in the same unit as the data [64].

$$MAE = \frac{1}{n}\sum_{i=1}^{n} |y_1 - \widehat{y_i}| \quad 6.5$$

- **Root Mean Squared Error (RMSE):** The RMSE metric is widely used for assessing the accuracy of a model prediction. It is the square root of the Mean Squared Error (MSE) and offers an estimation of the average magnitude of prediction errors in the same units as the original data. In simplified terms, RMSE provides an indication of the average gap between predictions and the actual values, with larger errors having a greater impact than in metrics such as MAE [64].

$$RMSE = \sqrt{\frac{1}{n}(\sum_{i=1}^{n}(y_1 - \widehat{y_i})^2)} \quad 6.6$$

6.6. Calculation of the energy output

One of the objectives of the study is to perform an energy assessment of both agrivoltaic (APV) systems and hypothetical non-APV systems. A temperature-corrected power equation (equation 6.7) [33] was utilized to accomplish this.

$$P_{temp} = P_{STC} * \left(1 + \gamma * (T_{mod} - T_{STC})\right) \quad 6.7$$

Where P_{temp} (W) represents the power output of the module, adjusted for temperature, at a specific module temperature , T_{mod} (℃) is the temperature of the module, P_{STC} (W) denotes the module power under standard test conditions (STC), the symbol γ (%/℃) indicates the temperature coefficient of power, while T_{STC} (℃) refers to the standard module temperature at STC, which is typically established at 25℃.

To find the temperature-corrected power output for the entire system, Equation 6.7 was modified to incorporate system capacity, as illustrated in Equation 6.8. Where the capacity of the Benin APV system was 15kWp.

$$P_{system} = P_{STC} * \left(1 + \gamma * (T_{mod} - T_{STC})\right) \quad 6.8$$

The equation was utilised at every time interval to forecast the temperature-adjusted power output for each group of module temperatures obtained from the three sets of coefficients: Faiman, Benin-tuned, and Büren-tuned.

The formula was applied at each time interval to predict the temperature-corrected power output of the systems. This was done for all the module temperature results derived from the three coefficients.

The calculation of energy generation was performed using Equation 6.9.

$$E_{mod} = \int P_{temp} * hours \quad 6.9$$

Where E_{mod} represents the energy produced during a specific timeframe in kWh, such as daily or monthly, P_{temp} represents the module power adjusted for temperature, while "hours" indicates the total duration in hours during which energy is calculated.

Given that the dataset was provided at 10-minute intervals, these intervals were converted to hours by dividing each 10-minute segment by 60 minutes per hour, yielding a factor of 0.167 hours.

The total system energy was calculated using Equation 6.10.

$$E_{system} = P_{system} * hours \quad 6.10$$

A poly silicon module with the following specifications was utilised for calculations related to both power and energy for the agrivoltaic and non-agrivoltaic systems.

- Poly Silicon module
  - Power = 255 W
  - Temperature coefficient = -0.4%/°C
  - Efficiency = 15 %
  - Area = 1.6 m^2

The datasheet is attached to appendix A.

6.7. Data analysis graphs

These performance of the two systems—agrivoltaic and non-agrivoltaic—was analysed and compared using Python scripts in a Kaggle notebook. The following evaluation metrics were employed.

Performance and comparative evaluation metrics

1. **Time Series Plots**

In order to identify seasonal patterns and trends, time series graphs were generated for ambient temperature, module temperatures, and energy outputs throughout the study period.

2. **Average monthly plots**

The demonstrate seasonal fluctuations and central tendencies, the mean module temperature and energy output of each system were depicted on a monthly basis.

3. **Daytime and Nighttime plots**

The ambient and module temperature data were categorized into daytime (6:00 AM to 6:00 PM) and nighttime (6:00 PM to 6:00 AM) intervals. The diurnal trends and patterns in temperature variation were analysed by plotting each subset separately. Furthermore, the system's efficacy during the crop growth period was evaluated by plotting daytime energy outputs on a monthly basis.

4. **Comparative analysis**

The thermal and energy performance of each system was assessed in a variety of conditions by comparing the mean temperatures and energy outputs of both systems over time.

5. **Scatter plots**

In order to facilitate a visual evaluation of the relationship between module temperature and energy yield, scatter plots were generated to illustrate the variation in energy output as a function of module temperature.

These analyses were performed on each module temperature dataset that was derived from the three heat transfer coefficients—Faiman, Benin-tuned, and Büren-tuned.

Chapter 7: Results and Discussion

7.1. Module temperature predictions for the non-agrivoltaic system – standard Faiman coefficients

As explained under section Chapter 5:, the module temperature for the non-agrivoltaic system was predicted using the meteorological ambient temperature obtained from solar GIS. This was done by applying the standard Faiman coefficients to the Faiman model using meteorological ambient temperature data as well as other parameters like POA and wind speed.

The plots for the module temperature variation over time, as well as daytime and nighttime averages are presented under subsection 7.2 together with the results from the agrivoltaic system.

7.2. Module temperature predictions for the agrivoltaic system using Faiman, Benin-tuned and Büren-tuned coefficients

Table 7.1 tabulates the values for the three heat transfer coefficients used in this study to predict the temperatures of the panels in Benin agrivoltaic system.

Table 7.1: Heat transfer coefficients utilised to predict the module temperature for the agrivoltaic system.

Heat transfer Coefficient	**U_0 (W/m²°C)**	**U_1 (W/m²°C)**
Standard Faiman	25	6.84
Benin-tuned	24.4	11.8
Büren-tuned	35.8	3.9

7.2.1. Module temperature results from standard Faiman heat transfer coefficients

The Faiman model was used to predict the temperature of PV modules in the agrivoltaic system by applying standard Faiman coefficients, as originally defined by Faiman [55]. These coefficients $U_0 = 25\ \mathrm{W/m^2°C}$ and $U_1 = 6.84\ \mathrm{W/m^2°C}$, were employed in conjunction with site-specific parameters. The microclimate ambient temperature, solar irradiance on the plane of array (POA), and wind speed values adjusted to a height of 2 meters were used to model the temperature for the agrivoltaic modules.

The temperature predictions for the agrivoltaic modules were subsequently compared to the estimated temperature of PV modules that would be expected if a conventional (non-agrivoltaic) PV system had been installed in the same region as the Benin agrivoltaic system. This comparison offers an understanding into the thermal behavior differences between the agrivoltaic and hypothetical non-agrivoltaic systems in similar climatic conditions.

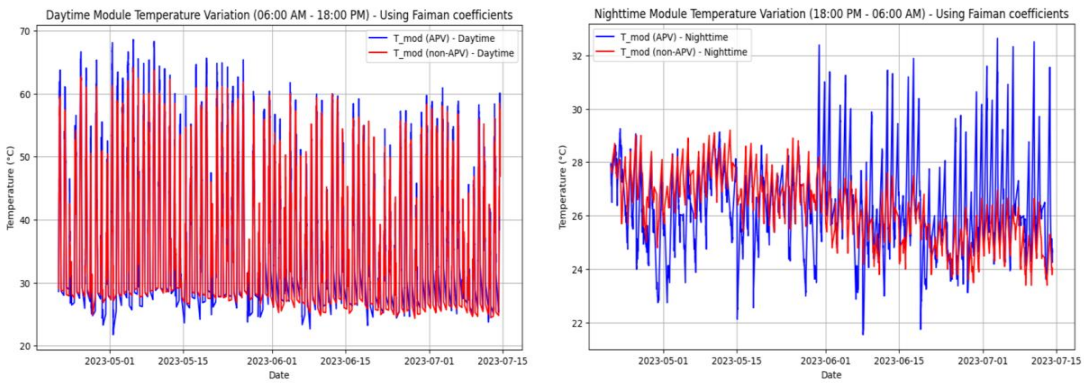

Figure 7.1:Daytime and nighttime module temperature variation over time using the standard Faiman heat transfer coefficients ($U_0 = 25\ W/m^2℃$ and $U_1 = 6.84\ W/m^2℃$). The blue plots represent the agrivoltaic module temperature values while the red plots are for the non-agrivoltaic module temperature values.

Figure 7.1 presents how the module temperature for the agrivoltaic system and non-agrivoltaic system fluctuate over the 83 days of the complete crop growth period. As it can be seen, the results show a similar trend to the results of the ambient temperature in Figure 6.1. The agrivoltaic module temperature fluctuates between 25℃ and 65℃ during the day while the non-agrivoltaic fluctuates between 25℃ and 60℃. In addition, solar panels in the agrivoltaic system show higher temperatures and lower temperatures compared to the solar panels in the non-agrivoltaic during the day as shown in Figure 7.2.

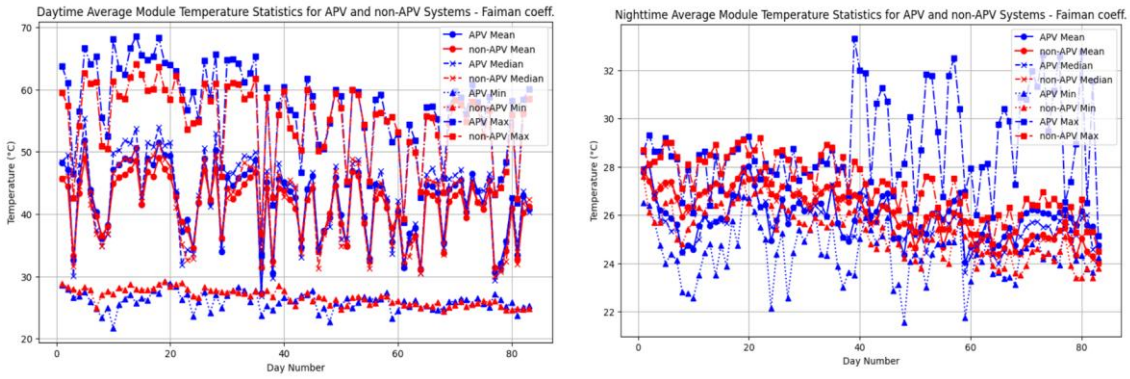

Figure 7.2:Variation of module temperature for the following statistical parameters: mean, median, minimum, and maximum values for daytime (left) and nighttime (right) values.

At night, on the hand, the solar modules in the agrivoltaic system experience the lowest temperature values for the first 40 days and later experienced high maximum temperatures from day 40 to day 83 of the crop growth period as clearly presented in Figure 7.2. The mean and median module temperature values for the two systems were comparable during the day. However, at night, the mean and median temperatures for agrivoltaic solar panels were noticeably low between day 0 and 40.

The agrivoltaic system exhibits increased temperature fluctuation, as evidenced by broader interquartile ranges (IQRs) and extended whiskers in the box plots (Figure 7.3 and Figure 7.4). This indicates that the microclimate formed beneath the PV modules in the agrivoltaic system experiences greater temperature variability. The non-agrivoltaic system exhibits comparatively more consistent temperatures, as anticipated, since it relies on meteorological data that reflect ambient conditions in open field.

The high daytime temperatures of the agrivoltaic system may result from heat retention beneath the PV modules. The modules capture solar radiation and obstruct wind flow,

resulting in a microclimate beneath the panels that experience higher temperatures compared to the open field conditions observed for the non-agrivoltaic system.

A further aspect contributing to elevated module temperatures is restricted heat dissipation within the agrivoltaic system. The agrivoltaic panels likely experience limited wind exposure because of their design and arrangement, which decreases convective cooling.

The higher nighttime module temperature in the agrivoltaic system may result from thermal inertia. The photovoltaic modules in the agrivoltaic system absorb heat during the day and gradually dissipate it at night. This results in the agrivoltaic system cooling at a slower rate than the non-agrivoltaic system.

The soil and crops beneath the agrivoltaic modules may facilitate heat retention, which is subsequently released gradually at night, so affecting the ambient temperature surrounding the modules. The non-agrivoltaic system, due to its increased exposure to open conditions, cools down more effectively at night because of enhanced wind exposure and reduced thermal mass relative to the agrivoltaic system.

The standard Faiman coefficients are site-and-installation-specific, thus, are likely not ideal for this analysis. To enhance precision, it is essential to conduct site-specific calibration of the Faiman coefficients, particularly in an Agrivoltaic configuration where the microclimate is influenced by elements such as shading, vegetation, and wind obstructions. Tuning U_0 and U_1 according to local conditions would probably yield a more precise depiction of the module temperatures. Therefore, in that regard, the Benin and Buren agrivoltaics-tuned coefficients were used to improve the precision of the results.

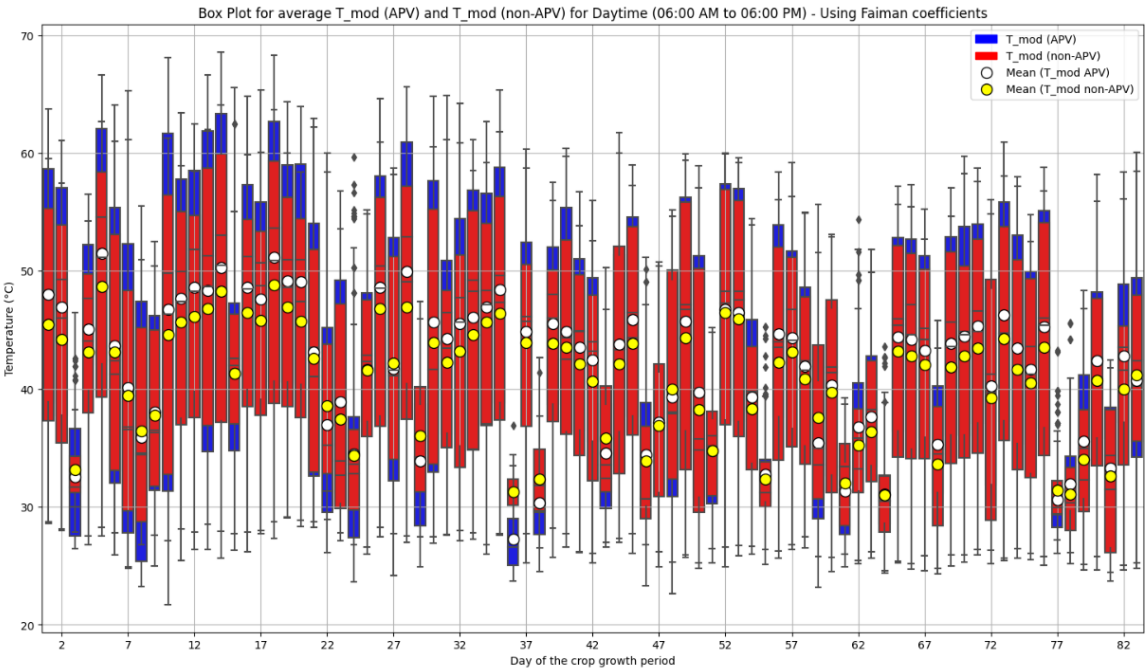

Figure 7.3: Box plot of the daytime average and mean module temperature variation over the 83 days of crop growth period using standard Faiman coefficients.

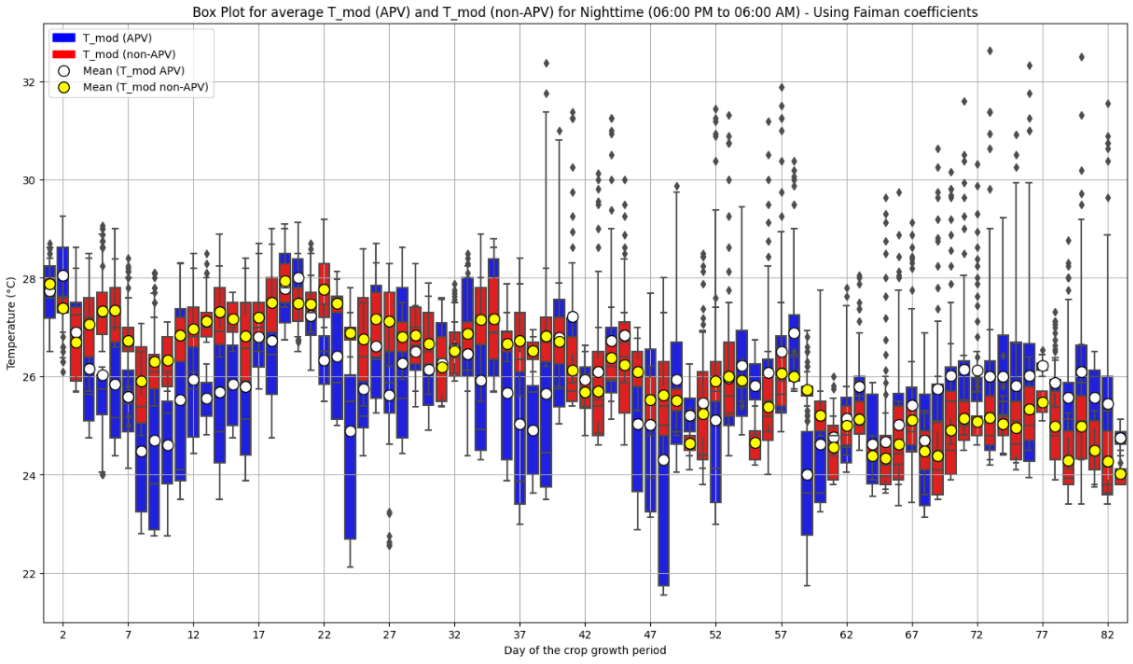

Figure 7.4: Box plot of the nighttime average and mean module temperature variation over the 83 days of crop growth period using standard Faiman coefficients.

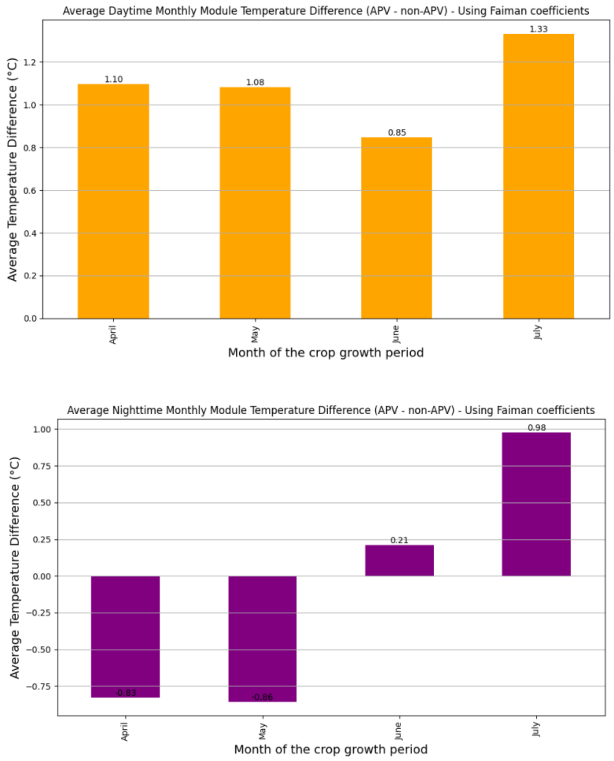

Figure 7.5: Average monthly daytime (yellow) and nighttime (purple) module temperature differences calculated as: agrivoltaic monthly average module temperature minus non-agrivoltaic monthly average module temperature ($T_{mod,\ agrivoltaic} - T_{mod,\ non\text{-}agrivoltaic}$).

As shown in Figure 7.5, the results of the standard Faiman coefficient did not show any cooling effect throughout the crop growth period. The temperature of the solar modules in the agrivoltaic system were all around 1℃ hotter than the modules in non-agrivoltaic system between the 21st April and 14th July 2023. However, April and May observed some cooling effect of over 0.75℃ during the night hours. While the night hours in the month of June and July did not record any cooling effect for the solar modules with the non-agrivoltaic system. The cooling effect at night in April and May can be attributed to the

low ambient temperatures for non-agrivoltaic system record for the two months as shown in Figure 7.5.

The elevated daytime temperatures of the agrivoltaic system may result from heat retention beneath the PV modules. The modules capture solar radiation and obstruct wind flow, resulting in a microclimate beneath the panels that experience higher temperatures compared to the open field conditions observed for the non-agrivoltaic system.

A further aspect contributing to elevated module temperatures is restricted heat dissipation within the agrivoltaic system. The agrivoltaic panels likely experience limited wind exposure because of their design and arrangement, which decreases convective cooling.

The higher nighttime module temperature in the agrivoltaic system may result from thermal inertia. The photovoltaic modules in the agrivoltaic system absorb heat during the day and gradually dissipate it at night. This results in the agrivoltaic system cooling at a slower rate than the non-agrivoltaic system.

The soil and crops beneath the agrivoltaic modules may facilitate heat retention, which is subsequently released gradually at night, so affecting the ambient temperature surrounding the modules. The non-agrivoltaic system, due to its increased exposure to open conditions, cools down more effectively at night because of enhanced wind exposure and reduced thermal mass relative to the agrivoltaic system.

The standard Faiman coefficients are site-and-installation-specific, thus, are likely not be ideal for this analysis. To enhance precision, it is essential to conduct site-specific calibration of the Faiman coefficients, particularly in an Agrivoltaic configuration where the microclimate is influenced by elements such as shading, vegetation, and wind

obstructions. Tuning U_0 and U_1 according to local conditions would probably yield a more precise depiction of the module temperatures. Therefore, in that regard, the Benin and Büren agrivoltaics-tuned coefficients were used to improve the precision of the results.

7.2.2. Benin heat transfer coefficient

The following section reveals the module temperatures for the agrivoltaic system, computed using coefficients specially obtained from the Benin dataset, in conjunction with the projected temperatures for an assumed non-agrivoltaic system. The coefficients specific to Benin were derived from local data gathered within the agrivoltaic system that cultivates multiple vegetables, thereby precisely representing the site's distinct characteristics.

As shown in Figure 7.6 the agrivoltaic system (blue) exhibit lower module temperatures than the non-agrivoltaic system (red) on most of the days during daytime hours. However, during the night hours, the agrivoltaic system show higher module temperatures for almost the entire period of crop growth.

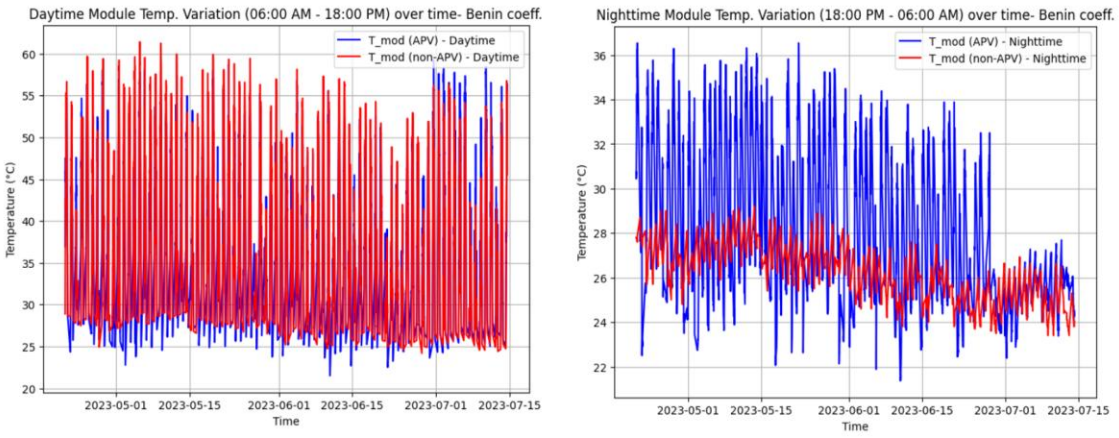

Figure 7.6: Daytime and nighttime module temperature variation over time using the Benin-tuned heat transfer coefficients ($U_0 = 24.4\ W/m^2°C$ *and* $U_1 = 11.8\ W/m^2°C$ *).*

The blue plots represent the agrivoltaic module temperature values while the red plots are for the non-agrivoltaic module temperature values.

In addition, Figure 7.7 show that the average module temperature (yellow dots) for the agrivoltaic system is generally lower, suggesting that Benin-derived coefficients result in a cooling effect during the day. However, the nighttime results indicate the opposite as Figure 7.8 presents.

During the day, the agrivoltaic system exhibits a narrower interquartile range (IQR) than the non-agrivoltaic system, indicating more uniform and stable module temperatures. The non-agrivoltaic system demonstrates greater temperature variability, characterized by more extreme temperature outliers and broader interquartile ranges, possibly attributable to elevated Faiman coefficient values that are not ideal for Benin's climate.

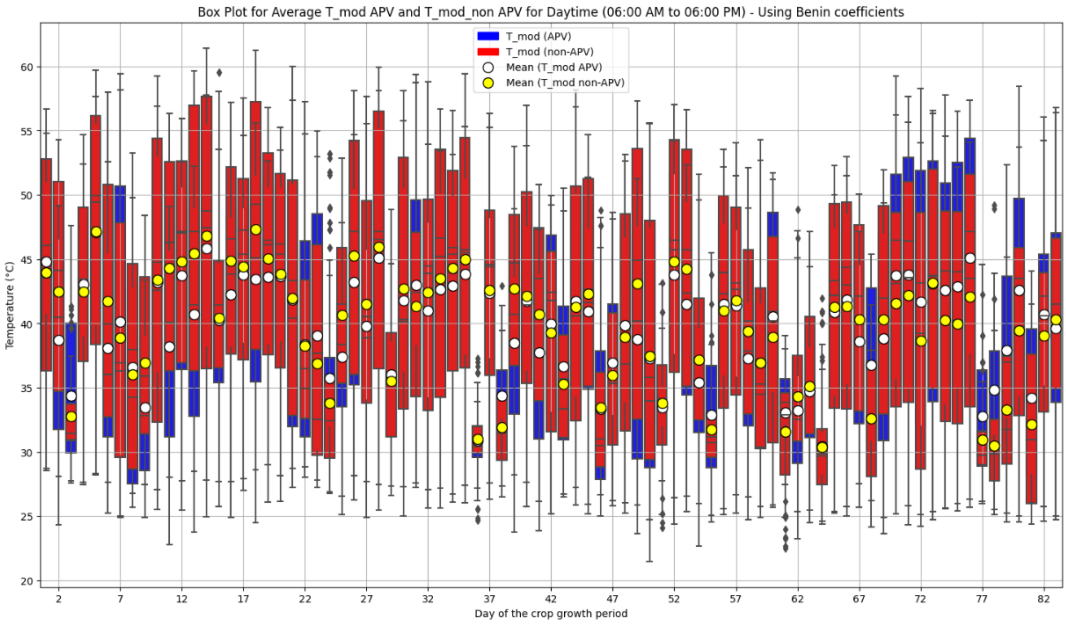

Figure 7.7: Box plots for 10-minutes averages for daytime module-temperature variation over the 83 days of crop growth period using Benin-tuned coefficients.

The Benin-derived coefficients effectively results in lower module temperature during the day, but not at night as shown in Figure 7.8.

Figure 7.9 also clearly demonstrates that during the day, the cooling effect of 0.22℃ to 1.03℃ was observed between April and June in the agrivoltaic system. However, in July there was no cooling effect at all. On the other hand, at night, the agrivoltaic system experienced higher temperatures than the non-agrivoltaic system between April to July.

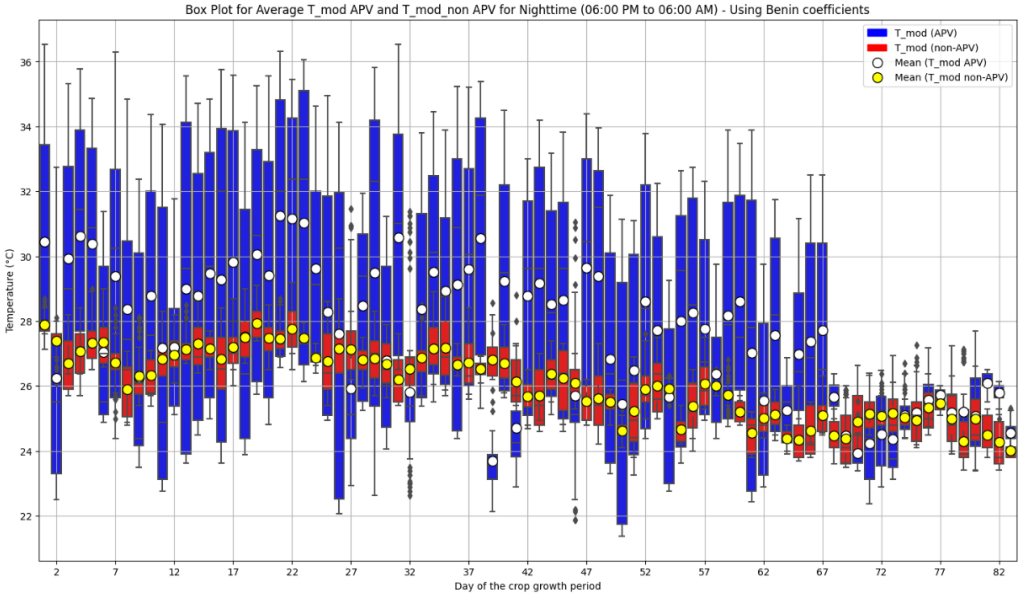

Figure 7.8: Box plots for 10-minutes averages for nighttime module-temperature variation over the 83 days of crop growth period using Benin-tuned coefficients.

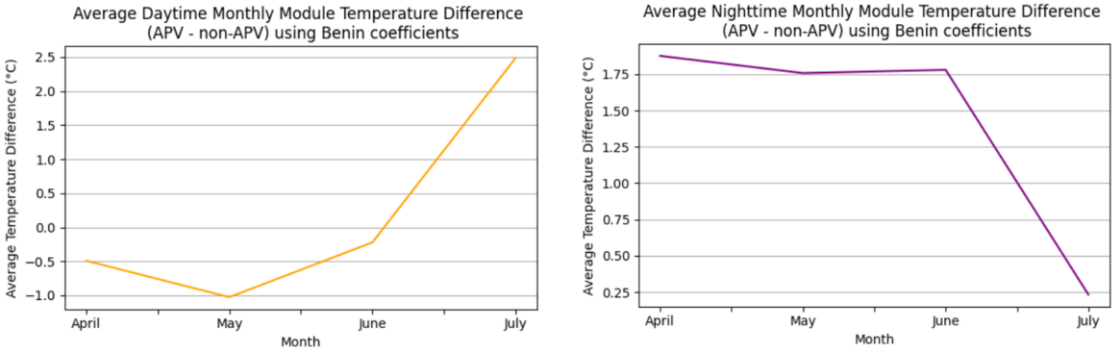

Figure 7.9: Average monthly daytime and nighttime module temperature differences calculated as: agrivoltaic monthly average module temperature minus non-agrivoltaic monthly average module temperature ($T_{mod,\ agrivoltaic} - T_{mod,\ non\text{-}agrivoltaic}$).

7.2.3. Büren heat transfer coefficient

Lastly, the Büren-derived coefficients, were utilised to forecast the thermal performance of solar panels in the Benin Agrivoltaic system. The derived coefficients were $U_0 = 24.4\ W/m^2℃$ and $U_1 = 11.8\ W/m^2℃$.

Unlike the results from the standard Faiman coefficients, Büren coefficients indicate a cooling effect in agrivoltaic solar modules for the entire crop growth period during the day. However, the nighttime results demonstrate that the module temperatures within the agrivoltaic system were significantly higher than in the non-agrivoltaic system. These can be observed in Figure 7.10.

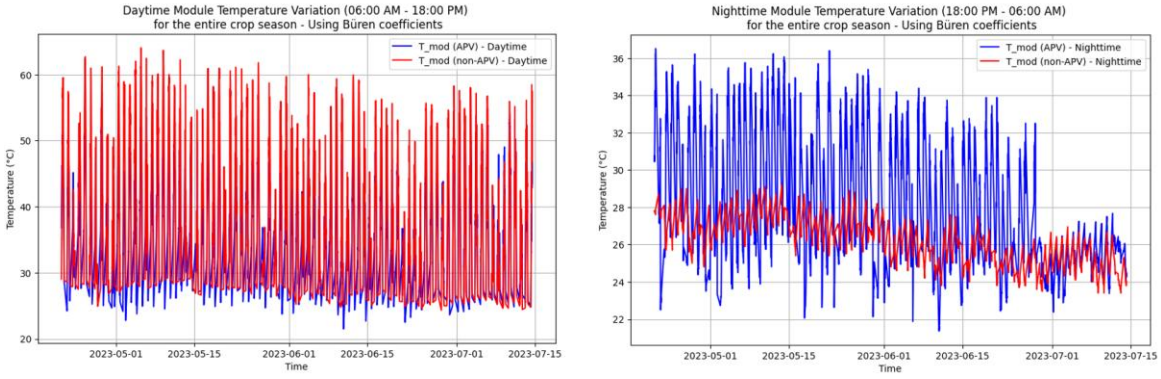

Figure 7.10: Daytime and nighttime module temperature variation over time using the Benin-tuned heat transfer coefficients ($U_0 = 24.4\ W/m^2℃$ and $U_1 = 11.8\ W/m^2℃$). The blue plots represent the Agrivoltaic module temperature values while the red plots are for the non-Agrivoltaic module temperature values.

In addition, Figure 7.11 indicate that the average module temperatures (yellow dots) for the agrivoltaic system are consistently lower, indicating that Büren coefficients forecast superior cooling for the agrivoltaic system, even in the hotter climate of Benin. However, the non-agrivoltaic system exhibits higher stability at night characterised by narrower

temperature fluctuations and overall lower temperatures, indicating cooling in the non-agrivoltaic system.

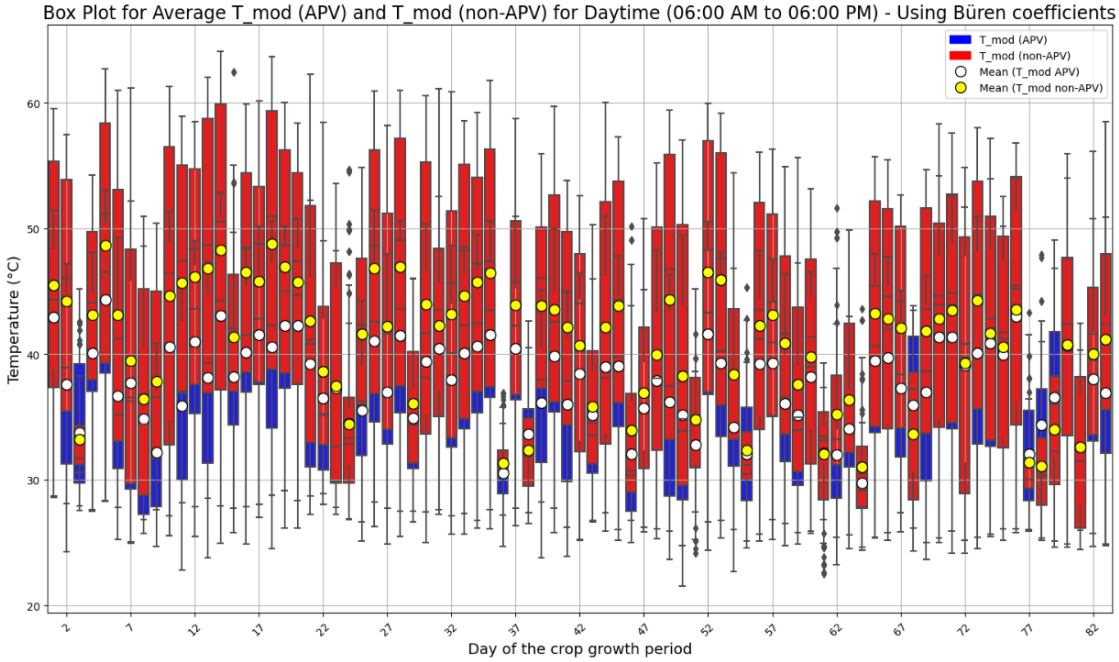

Figure 7.11: Box plot of the daily daytime average and mean module temperature variation over the 83 days of crop growth period using Büren -tuned coefficients.

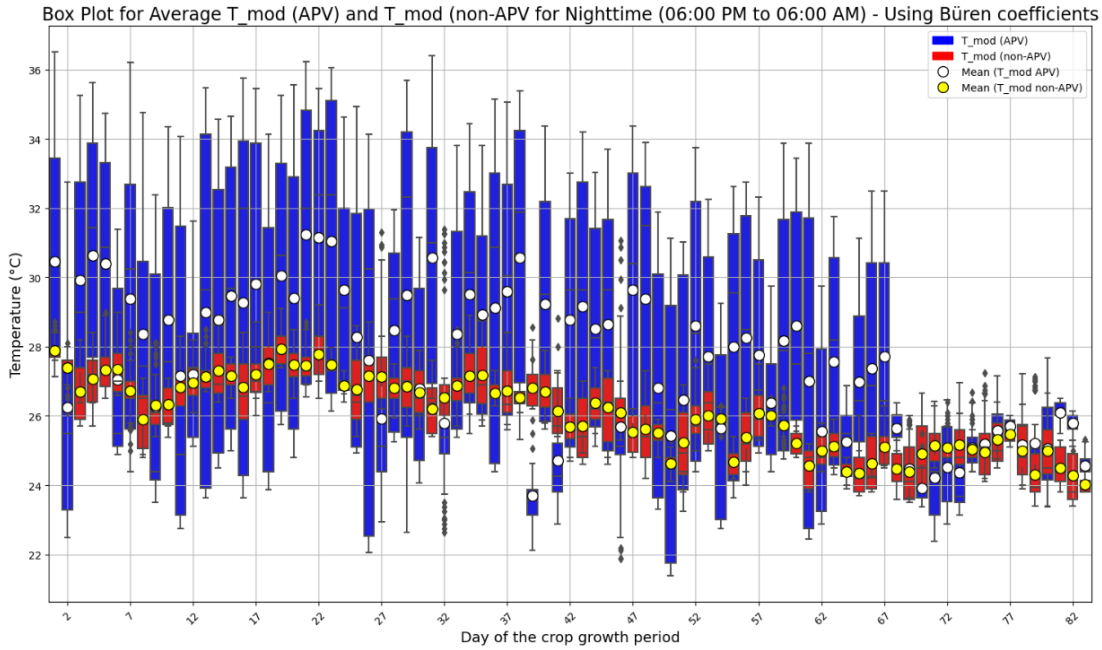

Figure 7.12: Box plot of the daily nighttime average and mean module temperature variation over the 83 days of crop growth period using Büren-tuned coefficients.

Overall, the Büren-derived coefficients resulted in cooler solar modules within the agrivoltaic system for the entire crop growth period as presented by negative module temperature differences in Figure 7.13. May appeared to have the highest cooling effect of 4.30℃, while July had the least cooling effect of 0.3℃. However, at night, the solar modules within the agrivoltaic system demonstrate high module temperature of over 1.75℃ for April to June, with the least difference of 0.23℃ to be in July.

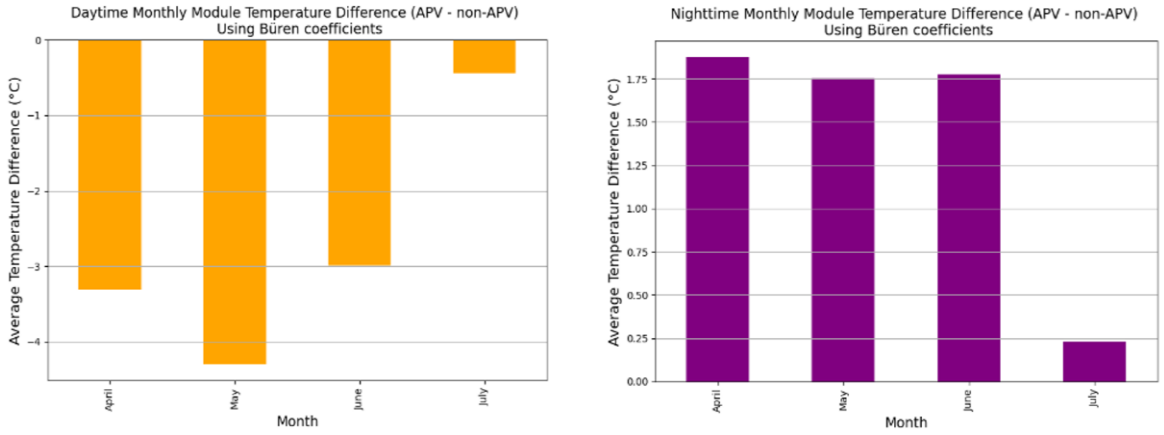

Figure 7.13: Average monthly daytime and nighttime module temperature differences calculated as: Agrivoltaic monthly average module temperature minus non-Agrivoltaic monthly average module temperature ($T_{mod,\ agrivoltaic} - T_{mod,\ non\text{-}agrivoltaic}$).

7.2.4. Summary of the module temperature differences.

Table 7.2: Average daytime monthly module temperature difference (agrivoltaic - non-agrivoltaic) for various heat transfer coefficients (U_0 and U_1) using Faiman Model

Months	T_mod (Faiman) ℃	T_mod (Benin) ℃	T_mod (Büren) ℃
April	1.10	-0.49	-3.31
May	1.08	-1.03	-4.30
June	0.85	-0.22	-2.99
July	1.33	2.48	-0.43

*Table 7.3: Daytime monthly % module temperature difference ((agrivoltaic - non-agrivoltaic)/non-agrivoltaic) *100% for various heat transfer coefficients (U_0 and U_1) using Faiman Model*

Months	T_mod (Faiman)	T_mod (Benin)	T_mod (Büren)
April	1.70%	-0.03%	-6.66%
May	1.68%	-0.20%	-8.29%
June	2.39%	-0.15%	-6.10%
July	3.70%	-0.00%	-0.16%

Table 7.4: Average-nighttime monthly module temperature difference (agrivoltaic - non-agrivoltaic) for various heat transfer coefficients (U_0 and U_1) using Faiman Model

Months	T_mod (Faiman) ℃	T_mod (Benin) ℃	T_mod (Büren) ℃
April	-0.83	1.88	1.87
May	-0.86	1.76	1.75
June	0.21	1.78	1.78
July	0.98	0.23	0.23

7.3. Assessment of the Energy output

Table 7.5: Average daytime monthly module energy difference (agrivoltaic - non-agrivoltaic)

Months	T_mod (Faiman) (kWh)	T_mod (Benin) (kWh)	T_mod (Büren) (kWh)
April	-25.3	12.3	58.2
May	-83.1	77.0	254.0
June	-23.8	31.1	163.3
July	-18.1	-39.1	22.3

*Table 7.6: Average daytime monthly % module energy difference ((agrivoltaic - non-agrivoltaic)/non-agrivoltaic) *100%*

Months	T_mod (Faiman)	T_mod (Benin)	T_mod (Büren)
April	- 1.07%	0.51%	2.46%
May	- 0.99%	0.91%	3.03%
June	- 0.32%	0.41%	2.19%
July	- 0.55%	-1.19%	0.68%

Table 7.5 above tabulates the average daytime energy differences between the agrivoltaic system and the non-AP system from April to July using three sets of heat transfer coefficients: Faiman, Benin and Büren. The energy difference was computed as follows:

Energy difference = Energy agrivoltaic system – Energy non-agrivoltaic system. The energy difference is presented in Table 7.6 as a percentage with reference to the Energy of the non-agrivoltaic system.

A positive energy differential (Energy_agrivoltaic > Energy_non-agrivoltaic) implies a cooling effect that led to increased energy output in the agrivoltaic system. In contrast, a negative value indicates that the agrivoltaic system produced less energy than the non-agrivoltaic system, possibly due to greater module temperatures in the agrivoltaic system.

Standard Faiman coefficients

- From April to June, the agrivoltaic system has a negative energy difference, with May having the highest difference of -83.1kWh. Thus, the solar modules in the agrivoltaic

system got hotter during these months which led to less energy being generated in comparison to the non-agrivoltaic system.

- In July, the energy difference is marginally negative (-18.1kWh), however, the decline is less pronounced than in May. This indicates a slight enhancement in the performance of the agrivoltaic system, potentially attributable to high solar irradiance during the month.

Benin coefficients

- In April, the agrivoltaic system produced slightly more energy than the non-agrivoltaic system (25kWh), likely due to early crop cooling.
- May, the energy difference increases to 77kWh, indicating the strong cooling effect which can be attributed to fully grown crops.
- The energy difference diminishes in June (31.1kWh), indicating a reduction in the cooling effect from May to June.
- In July, the Energy differential drops to -39.1kWh, indicating that there was no cooling effect in this month which could be due to higher temperatures in within the agrivoltaic system.

Büren coefficients

- The energy difference for Büren show a similar trend as the Benin-coefficient results. However, Büren results also demonstrate a positive energy difference in July of 22.3kWh which was negative for Benin coefficient.

- Therefore, Büren coefficient also reveal that the cooling affect was strong in May, as indicated by a positive difference of 254.0kWh. The effect of cooling slightly weakened from May to June (163.3) as shown in Table 7.5.
- In July, the impact of cooling strongly decreased but it was still observant as demonstrated by a low positive difference of 22.3kWh.

7.4. Scatter plots for the correlation between module temperature and energy yield

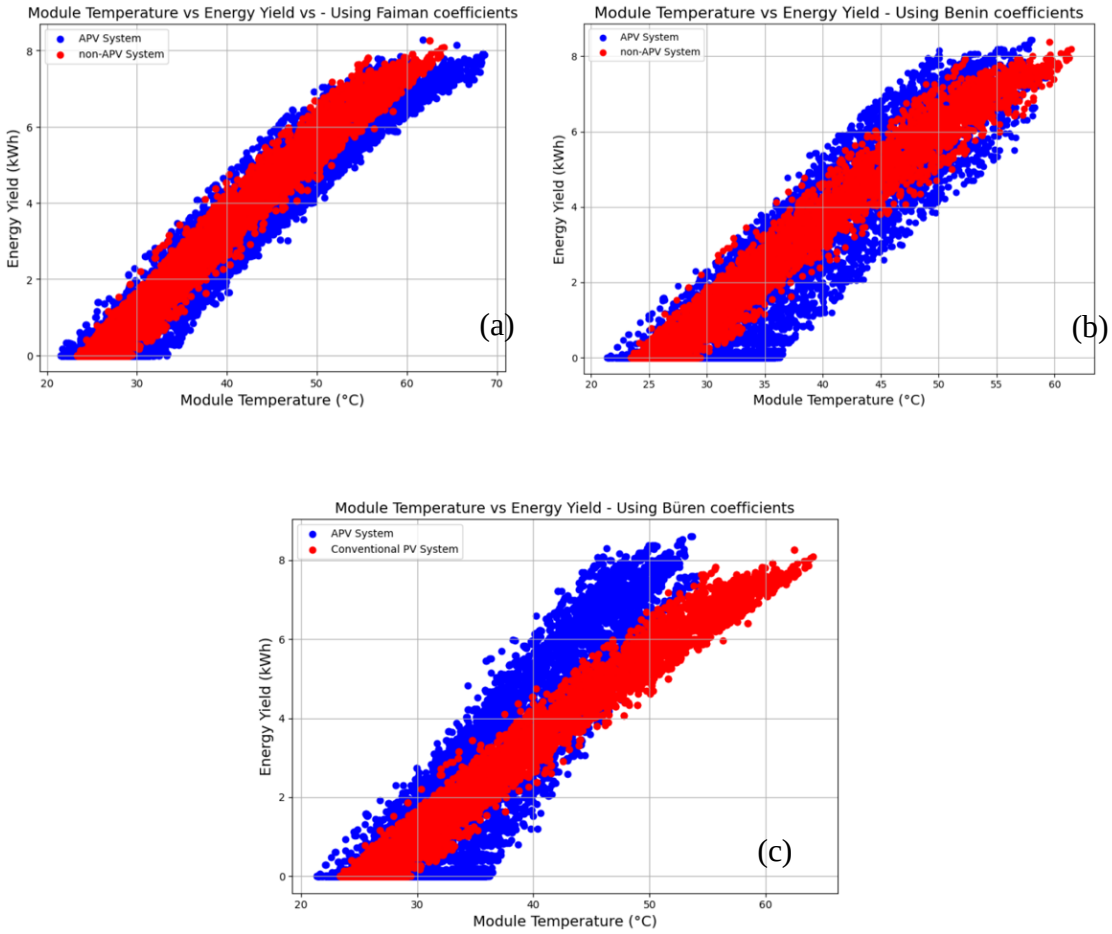

Figure 7.14: Energy output relative to module temperature for APV and non-APV systems utilising (a) standard Faiman coefficients, (b) Benin coefficients, and (c) Büren

coefficients, illustrating the influence of optimization on capturing cooling effects in AgriPV configurations.

The three graphs (a), (b), and (c) in Figure 7.14 depict the correlation between module temperature (computed using various heat transfer coefficients) and energy yield for APV (blue) and non-APV (red) systems. The temperature models depicted in each plot indicate that adjusting the heat transfer coefficients influences the discrepancies in energy production between APV and non-APV systems, underscoring the effect of certain climatic and configuration factors on PV performance.

- **Graph (a) - Faiman Standard Coefficients:** Utilizing the untuned standard Faiman coefficients, both APV and non-APV systems demonstrate comparable energy yield performance across the temperature spectrum, with a minor divergence between the two groups. The overlap in energy output indicates that the model may inadequately represent the particular cooling effects of the APV configuration, as the Faiman coefficients are generalized and may not accurately reflect the local variables pertinent to the APV environment.
- **Graph (b) - Benin Coefficients:** The Benin coefficients, obtained from the environmental data of an AgriPV system in Benin, enhance the distinction between APV and non-APV energy production. The APV system (blue) regularly demonstrates superior energy yield relative to the non-APV system (red) at comparable temperatures. The augmented separation indicates that the Benin coefficients more precisely reflect the cooling effect in the APV system, potentially enhanced by localized shade and microclimatic conditions resulting from crop transpiration. This

graph highlights how adapting the model to site-specific data might uncover energy yield benefits of the APV system.

- **Graph (c) - Buren Coefficients:** The Buren coefficients, obtained from data in a temperate environment AgriPV system in Buren, Germany, reveal a more pronounced distinction in energy yield between APV and non-APV systems, particularly at elevated module temperatures. The increased differentiation suggests that the Buren coefficients reflect a more pronounced cooling effect, probably attributable to variations in wind, crop density, and shade patterns in a temperate environment. The distinct disparity in energy output between APV and non-APV systems indicates that the precise adjustment of coefficients to align with local climatic circumstances facilitates a more accurate representation of the cooling benefits in AgriPV systems.

The study of these three graphs indicates that fine-tuning temperature prediction models with site-specific coefficients (Benin and Buren) yields a more precise representation of the energy output disparities between APV and non-APV systems. The generalized Faiman model inadequately captures these distinctions, suggesting that localized coefficients provide a more accurate comprehension of the cooling effects in APV systems and their influence on energy yield. This fine-tuning is essential for precisely assessing and enhancing the performance of AgriPV systems under varied climatic conditions.

7.5. Temperature variation

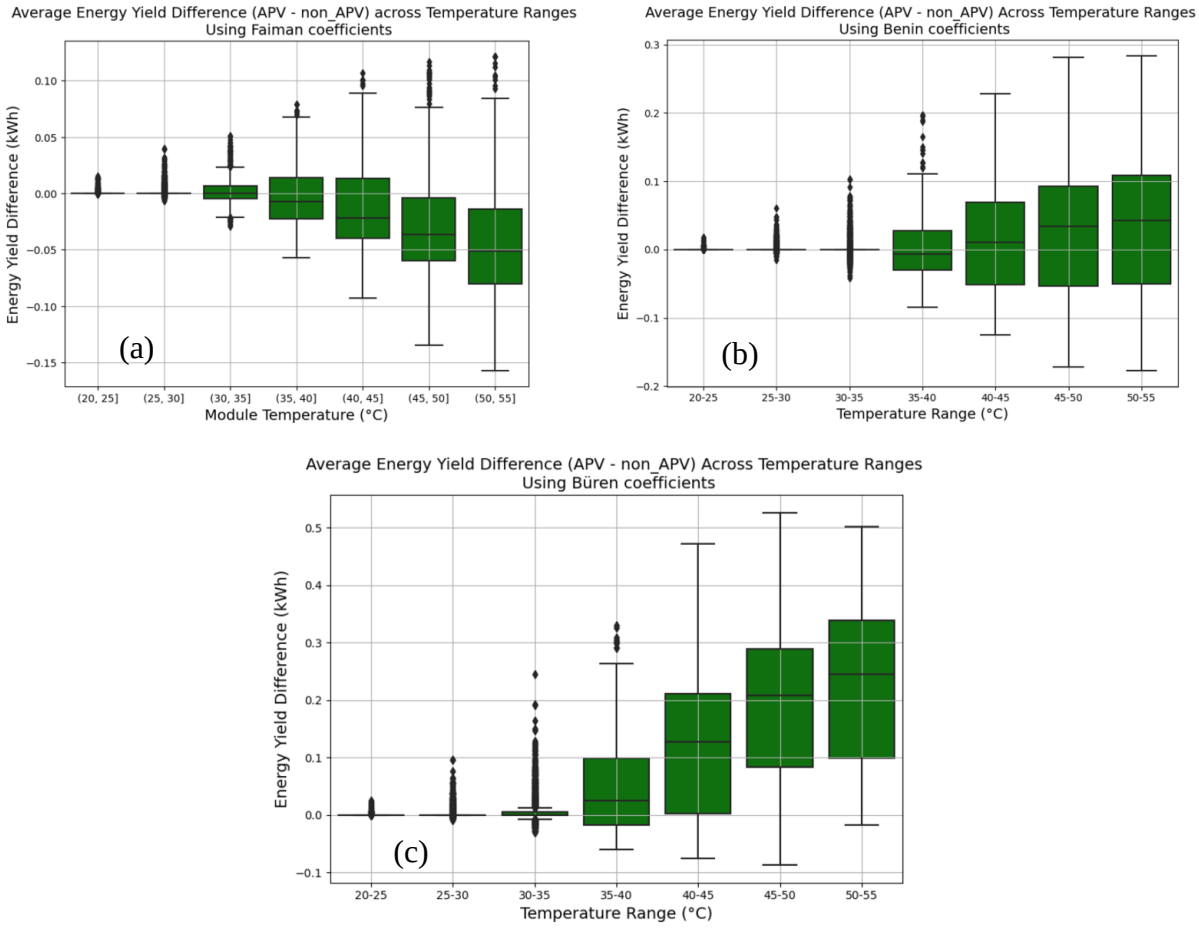

Figure 7.15: Variation of the difference in energy yield over different temperature ranges.

The graphs in Figure 7.15: illustrate the average energy yield difference over several temperature ranges utilising the results from standard Faiman, Benin and Büren coefficients. The Büren coefficients reveal a distinct trend in which the difference in energy yield is constantly positive, particularly at higher temperatures (exceeding 35℃), signifying a strong cooling effect that enables the agrivoltaic system to surpass the non-agrivoltaic system.

Conversely, the Faiman, Benin and Büren coefficients demonstrate larger variability, with some negative energy yield discrepancies at lower temperature ranges, indicating diminished cooling efficacy in the agrivoltaic system.

7.6. Correlation of the heat transfer coefficients

Table 7.7: Correlation of results obtained from Faiman and Büren coefficients to results obtained from Benin coefficient.

Comparison	**MAE (°C)**	**MSE (°C²)**	**RMSE (°C)**	**R²**
Benin (true) vs Faiman (pred)	0.540833	0.927247	0.962937	0.991693
Benin (true) vs Büren (pred)	0.972480	3.012090	1.735537	0.973017

Table 7.7: juxtaposes the precision of temperature estimates utilising the Faiman and Büren coefficient with the Benin-tuned coefficient derived from Benin-agrivoltaic-dataset (actual). The comparison between Benin and Faiman reveals reduced error metrics (MAE=0.54 ℃, RMSE=0.96 ℃ AND MSE=0.93 ℃) and elevated R^2 value of 0.99, signifying superior concordance with the authentic Benin data. The comparison between Benin and Büren exhibits higher error metrics MAE=0.97 ℃, RMSE=3.01 ℃ AND MSE=1.74 ℃) and elevated R^2 value of 0.98, indicating that Faiman coefficients align, ore closely with Benin data than with Büren coefficients. This suggest that although the Büren coefficients may be superior for cooling in energy yield assessments, the Faiman coefficients correspond more accurately with the actual temperature data from Benin.

Chapter 8: Summary for the discussion of the results

The effects of geographical location, weather conditions, crop growth seasons on the results

The agrivoltaic system in Benin, which cultivates a variety of vegetables during the crop season from 21st April to 14th July 2023, was the source of data for this study. The thermal performance of the PV modules could possibly be significantly influenced by several factors including but not limited to the geographical location, meteorological conditions and agricultural practices of Benin, thus these factors should be considered when interpreting the results.

1. Weather condition in Benin between April and July:

Benin has a tropical climate with a distinct wet season from April to October [65]. During the early rainy season, which spans from April to July, the data collection period is marked by warmer temperatures, humidity, and an increase in cloud cover as well as precipitation [66].

During this time (April to July), the daytime temperature can exceed 30°C, and the humidity levels are high [67]. The performance of both agrivoltaic and non-agrivoltaic systems can be substantially impacted by these conditions, as they reduce the effectiveness of convective cooling and increase the likelihood of heat retention in the modules, especially during the night.

The agrivoltaic system may have experienced a more pronounced cooling effect during the day due to the comparatively cooler period, particularly in April and May. The heat

dissipation from the PV modules may have been improved due to the combined effect of reduced air temperatures and the shade provided by the panels themselves.

The decreasing cooling effect observed in the agrivoltaic system is likely due to the increased humidity levels and rising temperatures in July [66], as the capacity of the module to dissipate heat reduces.

2. Geographical location

Benin is situated in the tropical zone at a latitude of around 6°N. The energy absorbed by the PV modules is influenced by the higher levels of solar irradiance that the country experiences throughout the entire the year [65].

During the period of April to July, the solar modules would be more susceptible to overheating during the day due to the increased heat burden caused by high GHI.

The effectiveness of wind-based cooling is restricted by the tropical conditions, which are characterised by high humidity and low wind speeds. This is particularly problematic in the agrivoltaic system, as the modules gradually release heat after sunset, contributing to nighttime heat retention.

3. The influence of vegetation and crop growth season

The mixed crops cultivated in the agrivoltaic system necessitate specific conditions to achieve optimal growth. The microclimate may have been influenced by the canopy of these crops, as it may have provided additional shading under the PV modules, thereby reducing the ambient temperature during the day.

The daytime cooling effect observed in April to June was likely influenced by the shading from the crops. The plants could have acted as a buffer against direct solar radiation, thereby reducing the heat burden on the solar panels.

The microclimatic cooling under the PV modules during the earlier months of the crop growth season may have been influenced by the increased soil moisture and evapotranspiration from the crops.

In addition, the crops would have reached maturity by July, resulting in higher biomass and more demand for water. As the air beneath the solar panels becomes saturated with moisture, it reduces the effectiveness of evapotranspiration as a cooling mechanism. This could be the reason for the reduced cooling effect within the agrivoltaic system for July.

4. Agricultural practices and seasonal variations

In Benin, rainfall is critical factor during the rainy season. As a result of the increased cloud cover and precipitation in May and June [65], the solar irradiance would have been reduced, resulting in lower temperatures and the potential to amplify the cooling effect in the agrivoltaic system. By July, however, when the precipitation would have somewhat lessened, module heating would have been made worse by more solar radiation.

The microclimate under the agrivoltaic system may have been affected by agricultural practices, such as irrigation. Consistent irrigation would have resulted in increased soil moisture, which would have contributed to cooling through evaporation. The evaporative cooling effect, however, may lessen during high-humidity months, which would further lessen the cooling that was observed in the month of July.

5. Thermal inertia

The agrivoltaic system retain more heat at night, as evidenced by the nighttime results. This could be attributed to the thermal inertia of both the PV modules and the impact of the microclimate in agrivoltaic systems. The likely cause of the temperature difference could be the transpiratory activity of plants beneath the PV modules, which absorb heat during the day and release it at night.

The effectiveness of the cooling mechanisms at night is reduced in tropical climates such as Benin, where diurnal temperature ranges (the difference between day and night temperatures) are smaller. This could be the reason why the agrivoltaic system has trouble dissipating heat at night, especially when the crops are more mature.

6. Microclimatic consequences of the Agrivoltaic system

The microclimate generated beneath the modules can have both beneficial and detrimental effects on crop growth. Although it is probable that crop heat stress may be mitigated by daytime cooling, the retention of heat during the night may result in a heated environment that impacts crop physiology. This equilibrium between heat retention and chilling is essential for comprehending the impact of the agrivoltaic system on agricultural productivity and PV efficiency.

Conclusion

The study evaluates the thermal and energy performance of photovoltaic modules in an Agrivoltaic system in Benin, employing three sets of heat transfer coefficients: Faiman, Benin and Büren. The findings indicated that the Büren coefficients consistently provided the strongest cooling effect, even though all coefficients showed some correlation between energy yield and module temperature. The agrivoltaic system in particular, demonstrated significantly lower temperatures and higher energy yield than the non-agrivoltaic system, especially at higher temperature ranges. The Faiman coefficients revealed minimal differences among the systems, suggesting a restricted capacity to reflect the cooling advantages of the agrivoltaic configuration. The Benin coefficients showed a moderate cooling effects that decreased during warmer months, indicating a need to for further adjustment to accurately represent local conditions.

In addition, statistical analysis of temperature predictions indicated that the standard Faiman coefficients were more closely aligned with the actual temperatures derived from Benin, whereas the Büren coefficients proved to be more effective in improving energy performance. This underscores the trade-off between precise temperature modelling and optimisation of cooling advantages.

The findings of the study highlight the necessity of employing site-specific heat-transfer coefficients and optimising system design, such as ventilation and module spacing, to improve the cooling effect tropical agrivoltaic systems.

Recommendations

Future studies could focus on enhancing temperature prediction models by integrating dynamic, site-specific environmental variables, including crop type, soil moisture, humidity, evapotranspiration, and local wind patterns. Conducting long-term studies in a variety of climates and AgriPV configurations would assist in the validation and generalization of the findings regarding the cooling effects of AgriPV systems in temperate and tropical regions. Subsequent investigations may examine hybrid cooling methodologies, using phase change materials (PCMs) or adjustable panel orientations, to improve module cooling and energy output. Examining the effects of various crop configurations and shading differences on microclimate development and photovoltaic performance may yield enhanced agricultural and energy outputs. Furthermore, integrating machine learning techniques for real-time parameter modifications and field validating temperature coefficients could greatly improve the predicted accuracy and adaptability of AgriPV models, offering a reliable tool for worldwide deployment.

References

[1] United Nations, World population projected to reach 9.8 billion in 2050, and 11.2 billion in 2100 | United Nations, 2024. https://www.un.org/ht/desa/world-population-projected-reach-98-billion-2050-and-112-billion-2100 (accessed 11 July 2024).

[2] International Energy Agency, World Energy Outlook 2022 (2022). https://ru.usembassy.gov/wp-content/uploads/sites/138/WorldEnergyOutlook20221.pdf. (accessed 29 March 2025).

[3] H. Hou, W. Lu, B. Liu, Z. Hassanein, H. Mahmood, S. Khalid, Exploring the Role of Fossil Fuels and Renewable Energy in Determining Environmental Sustainability: Evidence from OECD Countries, Sustainability 15 (2023) 2048. https://doi.org/10.3390/su15032048.

[4] IEA, Greenhouse Gas Emissions from Energy Data Explorer – Data Tools - IEA, 2023. https://www.iea.org/data-and-statistics/data-tools/greenhouse-gas-emissions-from-energy-data-explorer (accessed 11 July 2024).

[5] Hannah Ritchie, Max Roser, Sector by sector: where do global greenhouse gas emissions come from?, Our World in Data (2020). https://ourworldindata.org/ghg-emissions-by-sector. (accessed 29 March 2025).

[6] US EPA, Global Greenhouse Gas Overview | US EPA, 2024. https://www.epa.gov/ghgemissions/global-greenhouse-gas-overview (accessed 11 July 2024).

[7] IRENA, World Energy Transitions Outlook: 1.5°C Pathway (2021). https://www.irena.org/-/media/Files/IRENA/Agency/Publication/2021/Jun/IRENA_World_Energy_Transitions_Outlook_2021.pdf. (accessed 29 March 2025).

[8] International Energy Agency, Technology Roadmap Solar Photovoltaic Energy - 2014 edition (2014).

[9] A. Delichatsios, The Land Footprint of PV Solar (and Nuclear and Wind Power), 2022. https://medium.com/@alkidel/the-land-footprint-of-solar-and-nuclear-and-wind-power-b4a8b2c42ba9 (accessed 12 July 2024).

[10] D. Ketzer, Land Use Conflicts between Agriculture and Energy Production Systems Approaches to Allocate Potentials for Bioenergy and Agrophotovoltaics, 2020.

[11] G.A. Barron-Gafford, R.L. Minor, N.A. Allen, A.D. Cronin, A.E. Brooks, M.A. Pavao-Zuckerman, The Photovoltaic Heat Island Effect: Larger solar power plants increase local temperatures, Sci. Rep. 6 (2016) 35070. https://doi.org/10.1038/srep35070.

[12] M. Trommsdorff, S. Grube, T. Keinath, M. Hopf, C. Hermann, F. Schönberger, C. Gudat, A.T. Boggio, M. Gajewski, P. Högy, C. Rösch, J.V. Vollprecht, Agrivoltaics: Opportunities for Agriculture and the Energy Transition, third ed., Fraunhofer Institute for Solar Energy Systems ISE, 2024.

[13] K. Mertens, Photovoltaics: Fundamentals, technology and practice, Second edition, Wiley, Chichester, West Sussex, 2019.

[14] R.A. Messenger, A. Abtahi, Photovoltaic Systems Engineering, CRC Press, 2018.

[15] G.A. Barron-Gafford, M.A. Pavao-Zuckerman, R.L. Minor, L.F. Sutter, I. Barnett-Moreno, D.T. Blackett, M. Thompson, K. Dimond, A.K. Gerlak, G.P. Nabhan, J.E. Macknick, Agrivoltaics provide mutual benefits across the food–energy–water nexus in drylands, Nat Sustain 2 (2019) 848–855. https://doi.org/10.1038/s41893-019-0364-5.

[16] H. Marrou, L. Guilioni, L. Dufour, C. Dupraz, J. Wery, Microclimate under agrivoltaic systems: Is crop growth rate affected in the partial shade of solar panels?, Agricultural and Forest Meteorology 177 (2013) 117–132. https://doi.org/10.1016/j.agrformet.2013.04.012.

[17] H. Marrou, J. Wery, L. Dufour, C. Dupraz, Productivity and radiation use efficiency of lettuces grown in the partial shade of photovoltaic panels, European Journal of Agronomy 44 (2013) 54–66. https://doi.org/10.1016/j.eja.2012.08.003.

[18] H.J. Williams, K. Hashad, H. Wang, K. Max Zhang, The potential for agrivoltaics to enhance solar farm cooling, Applied Energy 332 (2023) 120478. https://doi.org/10.1016/j.apenergy.2022.120478.

[19] C. Dupraz, H. Marrou, G. Talbot, L. Dufour, A. Nogier, Y. Ferard, Combining solar photovoltaic panels and food crops for optimising land use: Towards new agrivoltaic schemes, Renewable Energy 36 (2011) 2725–2732. https://doi.org/10.1016/j.renene.2011.03.005.

[20] A. Goetzberger, A. Zastrow, On the Coexistence of Solar-Energy Conversion and Plant Cultivation, International Journal of Solar Energy 1 (1982) 55–69. https://doi.org/10.1080/01425918208909875.

[21] H. Dinesh, J.M. Pearce, The potential of agrivoltaic systems, Renewable and Sustainable Energy Reviews 54 (2016) 299–308. https://doi.org/10.1016/j.rser.2015.10.024.

[22] C. Dupraz, H. Marrou, G. Talbot, L. Dufour, A. Nogier, Y. Ferard, Combining solar photovoltaic panels and food crops for optimising land use: Towards new agrivoltaic schemes, Renewable Energy 36 (2011) 2725–2732. https://doi.org/10.1016/j.renene.2011.03.005.

[23] M. Trommsdorff, J. Kang, C. Reise, S. Schindele, G. Bopp, A. Ehmann, A. Weselek, P. Högy, T. Obergfell, Combining food and energy production: Design of an agrivoltaic system applied in arable and vegetable farming in Germany, Renewable and Sustainable Energy Reviews 140 (2021) 110694. https://doi.org/10.1016/j.rser.2020.110694.

[24] M. Trommsdorff, M. Vorast, N. Durga, S.M. Padwardhan, Potential of agrivoltaics to contribute to socio-economic sustainability: A case study in Maharashtra/India, in: agrivoltaicS2020 Conference: Launching Agrivoltaics World-wide, Perpignan, France, Online, AIP Publishing, 2021, p. 40001.

[25] S. Ravi, J. Macknick, D. Lobell, C. Field, K. Ganesan, R. Jain, M. Elchinger, B. Stoltenberg, Colocation opportunities for large solar infrastructures and agriculture in drylands, Applied Energy 165 (2016) 383–392. https://doi.org/10.1016/j.apenergy.2015.12.078.

[26] R. Kuleape, M. Berwind, S. Velez, B. Bingwa, F. Segbedji, M. Trommsdorff, A. Heimsath, M. Ploeg, W. Platzer, D. Bauknecht, H. Mbalundu, W. Amponsah, Assessing the Impact of Open Agrivoltaics on Microclimates by Modelling the Potential Heat Flux and Evapotranspiration, Freiburg, 2024. (preprint).

[27] D. Jung, F. Schönberger, F. Spera, Effects of Agrivoltaics on the Microclimate in Horticulture, AgriVoltaics Conf Proc 2 (2024). https://doi.org/10.52825/agripv.v2i.1033.

[28] S. Gorjian, E. Bousi, Ö.E. Özdemir, M. Trommsdorff, N.M. Kumar, A. Anand, K. Kant, S.S. Chopra, Progress and challenges of crop production and electricity generation in agrivoltaic systems using semi-transparent photovoltaic technology, Renewable and Sustainable Energy Reviews 158 (2022) 112126. https://doi.org/10.1016/j.rser.2022.112126.

[29] C.B. Honsberg, D.G. Bowden, Photovoltaics Education Website (2019).

[30] J.A. Duffie, W. Beckman, N. Blair, Solar Engineering of Thermal Processes, Photovoltaics and Wind, 5th Edition, fifthth ed., John Wiley et Sons, Incorporated, Newark, 2020.

[31] E. Türkdoğru, M. Kutay, Analysis of albedo effect in a 30-kW bifacial PV system with different ground surfaces using PVsyst software, Journal of Energy Systems 6 (2022) 543–559. https://doi.org/10.30521/jes.1105348.

[32] I. Yahyaoui (Ed.), Advances in renewable energies and power technologies, Elsevier, Amsterdam, 2018.

[33] J. Nelson, The physics of solar cells, Imperial College Press; Distributed by World Scientific Pub. Co, London, River Edge NJ, 2003.

[34] P. Würfel, U. Würfel, Physics of solar cells: From basic principles to advanced concepts, thirdrd edition, Wiley-VCH Verlag GmbH & Co. KGaA, Weinheim, druk 2023.

[35] A. Luque, S. Hegedus, Handbook of photovoltaic science and engineering, secondnd ed., Wiley, Chichester West Sussex U.K., 2011.

[36] M. Nicola, Modelling and Validating Heat Transfer Effects in Floating PV Installations. MSc Thesis, Fraunhofer Institute for Solar Energy (ISE), Freiburg University, 2023.

[37] National Renewable Energy Laboratory, NREL Best Research-Cell PV Efficiency Chart. https://www.nrel.gov/pv/cell-efficiency.html. (Accessed 29 March 2025).

[38] M.A. Green, Y. Hishikawa, E.D. Dunlop, D.H. Levi, J. Hohl-Ebinger, M. Yoshita, A.W. Ho-Baillie, Solar cell efficiency tables (Version 53), Progress in Photovoltaics 27 (2019) 3–12. https://doi.org/10.1002/pip.3102.

[39] C. Sun, Y. Zou, C. Qin, B. Zhang, X. Wu, Temperature effect of photovoltaic cells: a review, Adv Compos Hybrid Mater 5 (2022) 2675–2699. https://doi.org/10.1007/s42114-022-00533-z.

[40] S. McFadyen, Photovoltaic (PV) Panel - Performance Modelling, 2015. https://myelectrical.com/notes/entryid/257/photovoltaic-pv-panel-performance-modelling (accessed 29 July 2024).

[41] B. Limane, C. Ould-Lahoucine, S. Diaf, Modeling and simulation of the thermal behavior and electrical performance of PV modules under different environment and operating conditions, Renewable Energy 219 (2023) 119420. https://doi.org/10.1016/j.renene.2023.119420.

[42] I. Kurniawati, Y. Sung, A Review of Heat Dissipation and Absorption Technologies for Enhancing Performance in Photovoltaic–Thermal Systems, Energies 17 (2024) 1721. https://doi.org/10.3390/en17071721.

[43] I.O. Harmailil, S.M. Sultan, C.P. Tso, A. Fudholi, M. Mohammad, A. Ibrahim, A review on recent photovoltaic module cooling techniques: Types and assessment methods, Results in Engineering 22 (2024) 102225. https://doi.org/10.1016/j.rineng.2024.102225.

[44] L. Xu, W. Liu, H. Liu, C. Ke, M. Wang, C. Zhang, E. Aydin, M. Al-Aswad, K. Kotsovos, I. Gereige, A. Al-Saggaf, A. Jamal, X. Yang, P. Wang, F. Laquai, T.G. Allen, S. de Wolf, Heat generation and mitigation in silicon solar cells and modules, Joule 5 (2021) 631–645. https://doi.org/10.1016/j.joule.2021.01.012.

[45] S. Nižetić, A.M. Papadopoulos, E. Giama, Comprehensive analysis and general economic-environmental evaluation of cooling techniques for photovoltaic panels, Part I: Passive cooling techniques, Energy Conversion and Management 149 (2017) 334–354. https://doi.org/10.1016/j.enconman.2017.07.022.

[46] D. Sato, N. Yamada, Review of photovoltaic module cooling methods and performance evaluation of the radiative cooling method, Renewable and Sustainable Energy Reviews 104 (2019) 151–166. https://doi.org/10.1016/j.rser.2018.12.051.

[47] M.S. Abd-Elhady, Z. Serag, H.A. Kandil, An innovative solution to the overheating problem of PV panels, Energy Conversion and Management 157 (2018) 452–459. https://doi.org/10.1016/j.enconman.2017.12.017.

[48] A.H. Alami, Effects of evaporative cooling on efficiency of photovoltaic modules, Energy Conversion and Management 77 (2014) 668–679. https://doi.org/10.1016/j.enconman.2013.10.019.

[49] M. Ebrahimi, M. Rahimi, A. Rahimi, An experimental study on using natural vaporization for cooling of a photovoltaic solar cell, International Communications in Heat and Mass Transfer 65 (2015) 22–30. https://doi.org/10.1016/j.icheatmasstransfer.2015.04.002.

[50] S. Nižetić, E. Giama, A.M. Papadopoulos, Comprehensive analysis and general economic-environmental evaluation of cooling techniques for photovoltaic panels, Part II: Active cooling techniques, Energy Conversion and Management 155 (2018) 301–323. https://doi.org/10.1016/j.enconman.2017.10.071.

[51] A. Mahdavi, M. Farhadi, M. Gorji-Bandpy, A. Mahmoudi. A review of passive cooling of photovoltaic devices.2022.https://doi.org/10.1016/j.clet.2022.100579.

[52] A. Maleki, A. Haghighi, M. El Haj Assad, I. Mahariq, M. Alhuyi Nazari, A review on the approaches employed for cooling PV cells, Solar Energy 209 (2020) 170–185. https://doi.org/10.1016/j.solener.2020.08.083.

[53] D.P.N. Nguyen, K. Neyts, J. Lauwaert, Proposed Models to Improve Predicting the Operating Temperature of Different Photovoltaic Module Technologies under Various Climatic Conditions, Applied Sciences 11 (2021) 7064. https://doi.org/10.3390/app11157064.

[54] M. Nicola, M. Berwind, Improving Module Temperature Prediction Models for Floating Photovoltaic Systems: Analytical Insights from Operational Data Analytical Insights from Operational Data. Fraunhofer Institute for Solar Energy Systems (2024). (preprint).

[55] D. Faiman, Assessing the outdoor operating temperature of photovoltaic modules, Progress in Photovoltaics 16 (2008) 307–315. https://doi.org/10.1002/pip.813.

[56] D.L. King, W.E. Boyson, J.A. Kratochvil, Photovoltaic Array Performance Model. Photovoltaic System R&D Department. Sandia National Laboratories. Report. (2004). https://www.osti.gov/servlets/purl/919131.

[57] D. Dirnberger, B. Müller, C. Reise, PV module energy rating: opportunities and limitations, Progress in Photovoltaics 23 (2015) 1754–1770. https://doi.org/10.1002/pip.2618.

[58] PVSystem — pvlib python 0.11.0 documentation, 2024. https://pvlib-python.readthedocs.io/en/stable/user_guide/pvsystem.html (accessed 28 July 2024).

[59] E. Skoplaki, A.G. Boudouvis, J.A. Palyvos, A simple correlation for the operating temperature of photovoltaic modules of arbitrary mounting, Solar Energy Materials and Solar Cells 92 (2008) 1393–1402. https://doi.org/10.1016/j.solmat.2008.05.016.

[60] E.Y. Rakhimov, N.R. Avezova, S. Emamgholizadeh, M. Ziaii, Assessment of the Technical Potential of PV Stations on the Example of the Fergana Valley. Part II: Analysis of Sunny, Partly Cloudy, and Cloudy Days, Appl. Sol. Energy 60 (2024) 346–356. https://doi.org/10.3103/S0003701X24602199.

[61] Songhaï – L'Afrique relève la tête !, 2024. https://songhai.org/ (accessed 21 October 2024).

[62] Windenergie-Daten der Schweiz, 2024. https://wind-data.ch/tools/profile.php?lng=en (accessed 21 October 2024).

[63] J. Nocedal, S.J. Wright, Numerical optimization, secondnd ed., Springer, New York, 2006.

[64] R. Barlow, Statistics: A guide to the use of statistical methods in the physical sciences, Wiley, Chichester England, New York, 1989.

[65] Benin Climate Zone, Weather By Month and Historical Data, 2024. https://weatherandclimate.com/benin (accessed 21 October 2024).

[66] Climate and Weather in Benin | Trip Report, 2024. https://www.tripreport.com/countries/benin/climate (accessed 21 October 2024).

[67] Jeroen en Dimi, Benin climate info | what's the weather like in Benin, 2024. https://www.whatstheweatherlike.org/benin/ (accessed 21 October 2024).

Appendix A: Ethical Clearance Certificate

UNAM
UNIVERSITY OF NAMIBIA

ETHICAL CLEARANCE CERTIFICATE

Ethical Clearance Reference Number: SOS-0231 **Date: 23AUGUST 2024**

This Ethical Clearance Certificate is issued by the University of Namibia Ethics Committee (REC) in accordance with the University of Namibia's Research Ethics Policy and Guidelines. Ethical approval is given in respect of undertakings contained in the Research Project outlined below. This Certificate is issued on the recommendations of the ethical evaluation done by the ethics committee.

Title of Project:	AN ASSESSMENT OF THE THERMAL AND ELECTRICAL PERFORMANCE OF AGRIPV IN ARID CLIMATES APPROACH
Student:	MS. HERTHA MBALUNDU
Student Number:	201704841
Supervisor(s):	DR. PETJA DOBREVA DR. MATTHEW BERWIND

Centre for Research Services

Take note of the following:

1. Any significant changes in the conditions or undertakings outlined in the approved Proposal must be communicated to the ethics committee. An application to make amendments may be necessary.
2. Any breaches of ethical undertakings or practices that have an impact on ethical conduct of the research must be reported to the ethics committee.
3. The Principal Researcher must report issues of ethical compliance to the ethics committee (through the Chairperson) at the end of the Project or as may be requested by the ethics committee.
4. The ethics committee retains the right to:

i) Withdraw or amend this Ethical Clearance if any unethical practices (as outlined in the Research Ethics Policy) have been detected or suspected,

ii) Request for an ethical compliance report at any point during the course of the research.

The ethics committee wishes you the best in your research.

Prof. Ezekeil Gwinyai Kwembeya (Chairperson Ethics Committee)

Prof. Davis Mumbengegwi (Head, Multidisciplinary Research)

Appendix B: Research Permission Letter

CENTRE FOR RESEARCH SERVICES
Office of the Pro-Vice Chancellor: Research, Innovation & Development
University of Namibia, Private Bag 13301, Windhoek, Namibia
340 Mandume Ndemufayo Avenue, Pioneers Park, Office F223 - Fblock, Second Floor
☎ +264 61 206 4673; E-mail:kmbulu@unam.na; URL.: http//www.unam.edu.na

UNAM
UNIVERSITY OF NAMIBIA

RESEARCH PERMISSION LETTER

Date: 29/10/2024

Student Name: HERTHA MBALUNDU

Student Number: 201704841

Programme: Master of Science in Renewable Energy

Approved Research Title: AN ASSESSMENT OF THE THERMAL AND ELECTRICAL PERFORMANCE OF AGRIPV IN ARID CLIMATES APPROACH

TO WHOM IT MAY CONCERN:

I hereby confirm that the above-mentioned student is registered at the University of Namibia for the programme indicated. The proposed study met all the requirements as stipulated in the University guidelines and has been approved by the relevant committees.

The proposal adheres to ethical principles as per attached Ethical Clearance Certificate. Permission is hereby granted to carry out the research as described in the approved proposal.

Best Regards

Dr. AEE Shikongo
Head: Postgraduate Research Support Services
Tel: +264 61 206 3129
E-mail: aeshikongo@unam.na

CENTRE FOR RESEARCH SERVICES
Office of the Director
2024 -10- 29
University of Namibia
UNAM

Appendix C: Module Data Sheet

Sunmodule™

SW 245 poly / Version 2.0 and 2.5 Frame

World-class quality
Fully-automated production lines and seamless monitoring of the process and material ensure the quality that the company sets as its benchmark for its sites worldwide.

SolarWorld Plus-Sorting
Plus-Sorting guarantees highest system efficiency. SolarWorld only delivers modules that have greater than or equal to the nameplate rated power.

25 years linear performance guarantee and extension of product warranty to 10 years
SolarWorld guarantees a maximum performance degression of 0.7% p.a. in the course of 25 years, a significant added value compared to the two-phase warranties common in the industry. In addition, SolarWorld is offering a product warranty, which has been extended to 10 years.*

*in accordance with the applicable SolarWorld Limited Warranty at purchase.
www.solarworld.com/warranty

Qualified, IEC 61215
Safety tested, IEC 61730
Periodic Inspection
1)

ISO 9001
ISO 14001
Certified

Intertek

US LISTED
Photovoltaic Module / Panel

Made in USA

SOLARWORLD

We turn sunlight into power.

www.solarworld.com

Sunmodule™

SW-02-5009US 08-2011

ecoDIRECT
CLEAN ENERGY SOLUTIONS

SW 245 poly / Version 2.0 and 2.5 Frame

PERFORMANCE UNDER STANDARD TEST CONDITIONS (STC)*

		SW 245
Maximum power	P_{max}	245 Wp
Open circuit voltage	V_{oc}	37.5 V
Maximum power point voltage	V_{mpp}	30.8 V
Short circuit current	I_{sc}	8.49 A
Maximum power point current	I_{mpp}	7.96 A

*STC: 1000W/m², 25°C, AM 1.5

PERFORMANCE AT 800 W/m², NOCT, AM 1.5

		SW 245
Maximum power	P_{max}	176.4 Wp
Open circuit voltage	V_{oc}	33.7 V
Maximum power point voltage	V_{mpp}	27.7 V
Short circuit current	I_{sc}	6.84 A
Maximum power point current	I_{mpp}	6.37 A

Minor reduction in efficiency under partial load conditions at 25°C: at 200W/m², 95% (+/-3%) of the STC efficiency (1000 W/m²) is achieved.

THERMAL CHARACTERISTICS

NOCT	46 °C
TC I_{sc}	0.034 %/K
TC V_{oc}	-0.34 %/K
TC P_{mpp}	-0.48 %/K
Operating range	-40°C to 90°C

IV-curves for SolarWorld Sunmodule Plus SW 245 poly at 25°C cell temperature

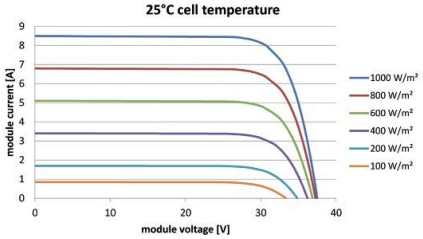

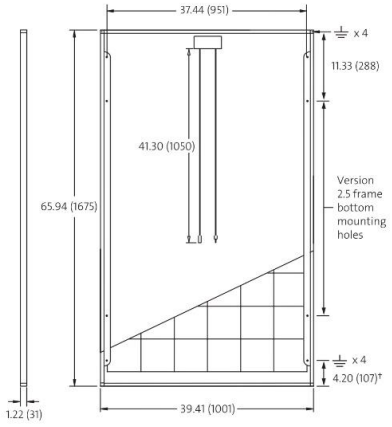

COMPONENT MATERIALS

Cells per module	60
Cell type	Poly crystalline
Cell dimensions	6.14 in x 6.14 in (156 mm x 156 mm)
Front	tempered glass (EN 12150)
Frame	Aluminum
Weight	46.7 lbs (21.2 kg)
UL Maximum Test Load**	50 psf (2.4kN/m²)
IEC Maximum Snow Test Load**	113 psf (5.4kN/m²)

**Please apply the appropriate factors of safety according to the test standard and local building code requirements when designing a PV system.

SYSTEM INTEGRATION PARAMETERS

Maximum system voltage SC II	1000 V
Max. system voltage USA NEC	600 V
Maximum reverse current	16 A
Max. mechanical load	5.4 kN/m²
Number of bypass diodes	3

ADDITIONAL DATA

Measuring tolerance[2]	+/- 3 %
SolarWorld Plus-Sorting[3]	$P_{Flash} \geq P_{max}$
Junction box	IP66
Connector	MC4
Module efficiency	14,6 %
Fire rating (UL 790)	Class C

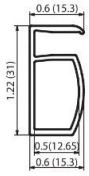

VERSION 2.0 FRAME
- Compatible with "Top-Down" mounting methodes
- Grounding Locations: 4 corners of the frame

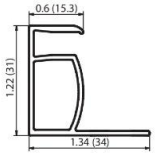

VERSION 2.5 FRAME
- Compatible with both "Top-Down" and "Bottom" mounting methodes
- Grounding Locations:
  - 4 corners of the frame
  - 4 locations along the length of the module in the extended flange†

1) Sunmodules dedicated for the United States and Canada are tested to UL 1703 Standard and listed by a third party laboratory. The laboratory may vary by product and region. Check with your SolarWorld representative to confirm which laboratory has a listing for the product.
2) Measuring tolerance is used conjunctions with the SolarWorld Limited Warranty. SolarWorld AG reserves the right to make specification changes without notice.
3) The output identified by SolarWorld (P_{Flash}) is always higher than the nominal output (P_{max}) of the module. PFlash is the power rating flashed at a SolarWorld manufacturing facility.
4) All units provided are imperial. SI units provided in parentheses.

Appendix D: List of nomenclature

Abbreviations

AgriPV	Agrivoltaics
APV	Agri-PV (Agricultural Photovoltaics)
DHI	Diffuse Horizontal Irradiance
DNI	Direct Normal Irradiance
FF	Fill Factor (dimensionless)
GHI	Global Horizontal Irradiance
GH	Green Hydrogen
IEA	International Energy Agency
LER	Land Equivalent Ratio
NOCT	Nominal Operating Cell Temperature
PCMs	Phase Change Materials
PERC	Passivated Emitter and Rear Cell
PV	Photovoltaic
SDGs	Sustainable Development Goals
V_{OC}	Open-Circuit Voltage
WS	Wind Speed

Y4GH2	Youth for Green Hydrogen

Acronyms

IRENA	International Renewable Energy Agency
JCol	Joint Communique of Intent
SASSCAL	Southern African Science Service Centre for Climate Change and Adaptive Land Management

Symbols

E_{ph}	Photon energy (J)
GHI	Global Horizontal Irradiance (W/m²)
DNI	Direct Normal Irradiance (W/m²)
DHI	Diffuse Horizontal Irradiance (W/m²)
T_{mod}	Module temperature (°C)
T_{amb}	Ambient temperature (°C)
NOCT	Nominal Operating Cell Temperature (°C)
I_{sc}	Short-Circuit Current (A)
V_{oc}	Open-Circuit Voltage (V)
P_{mpp}	Maximum Power Point (W)

I	Current (A)
V	Voltage (V)
η	Efficiency (%)
α	Temperature coefficient of current
β	Temperature coefficient of voltage

Subscripts

amb	Ambient
mod	Module
APV	AgriPV (agrivoltaic) System
non-APV	non-AgriPV (non-agrivoltaic) system
NOCT	Nominal Operating Cell Temperature